The Astrophysical Journal, 688:437–455, 2008 November 20

X-RAY FLARES IN ORION YOUNG STARS. II. FLARES, MAGNETOSPHERES, AND PROTOPLANETARY DISKS

Konstantin V. Getman,[1] Eric D. Feigelson,[1] Giusi Micela,[2] Moira M. Jardine,[3] Scott G. Gregory,[3] and Gordon P. Garmire[1]

Received 2008 March 25; accepted 2008 July 17

ABSTRACT

We study the properties of powerful X-ray flares from 161 pre-main-sequence (PMS) stars observed with the *Chandra X-ray Observatory* in the Orion Nebula region. Relationships between flare properties, protoplanetary disks, and accretion are examined in detail to test models of star-disk interactions at the inner edge of the accretion disks. Previous studies found no differences in flaring between disk-free and accreting systems other than a small overall diminution of X-ray luminosity in accreting systems. The most important finding is that X-ray coronal extents in fast-rotating disk-free stars can significantly exceed the Keplerian corotation radius, whereas X-ray loop sizes in disky and accreting systems do not exceed the corotation radius. This is consistent with models of star-disk magnetic interaction in which the inner disk truncates and confines the PMS stellar magnetosphere. We also find two differences between flares in accreting and disk-free PMS stars. First, a subclass of superhot flares with peak plasma temperatures exceeding 100 MK are preferentially present in accreting systems. Second, we tentatively find that accreting stars produce flares with shorter durations. Both results may be consequences of the distortion and destabilization of the stellar magnetosphere by the interacting disk. Finally, we find no evidence that any flare types, even slow-rise top-flat flares, are produced in star-disk magnetic loops. All are consistent with enhanced solar long-duration events with both footpoints anchored in the stellar surface.

Subject headings: open clusters and associations: individual (Orion Nebula Cluster) — planetary systems: protoplanetary disks — stars: flare — stars: magnetic fields — stars: pre–main-sequence — X-rays: stars

1. INTRODUCTION

A broad consensus has emerged in the past decade concerning the structure and astrophysics of pre-main-sequence (PMS) stars. The angular momentum inherited from the collapsing interstellar material is mostly distributed into a rapidly rotating protostar, a Keplerian protoplanetary disk, and frequently the orbital motion of multiple stellar components. The young star interacts with its disk in a complex fashion, with accretion and ejection of collimated outflow. It is widely believed that strong magnetic fields generated within the young star mediate this star-disk interaction, truncating the disk and funneling accretion onto limited portions of the stellar surface. These issues are developed in a variety of reviews (e.g., Hartmann 1998; Bouvier et al. 2007; Bouvier & Appenzeller 2007).

It has been difficult, however, to elucidate in detail the nature of the PMS stellar magnetospheres and their role in facilitating star-disk interactions and accretion. Well-developed analytical theory assumes that a dipolar field extends to several stellar radii where the Keplerian orbits and stellar fields are in corotation, that it interacts with the disk magnetic field, and that it guides accretion both onto the surface and into a high-velocity collimated outflow (e.g., Shu et al. 1994; Lovelace et al. 1995). However, considerable evidence has emerged that the magnetic fields on the surfaces of PMS stars are concentrated in complex multipolar active regions similar to those on the Sun, rather than forming a simple dipolar. This emerges from photometric imaging, Doppler imaging, circular polarization, and spectroscopy of Zeeman-sensitive lines from PMS photospheres (e.g., Daou et al. 2006; Yang et al. 2007; Johns-Krull 2007; Donati et al. 2007). Recently, theoretical efforts have begun to calculate the resulting complex PMS magnetosphere and accretion process (Jardine et al. 2006; Gregory et al. 2006b; Long et al. 2007).

X-ray studies are a potentially useful tool for investigating these issues. It has long been known that late-type stars exhibit their highest levels of X-ray emission, arising mostly from violent magnetic reconnection events, during their PMS phase (see, e.g., reviews by Feigelson & Montmerle 1999; Feigelson et al. 2007). Recent X-ray surveys of nearby PMS stellar populations give detailed insights into PMS magnetic flaring; these include the *Chandra* Orion Ultradeep Project (COUP; Getman et al. 2005) and the *XMM-Newton* Extended Survey of Taurus (XEST; Güdel et al. 2007). Astrophysical study of the properties of individual flares and statistical study of many flares, from both the COUP and XEST observations, reveal that most events are similar to solar magnetic flaring, but with X-ray luminosities enhanced by a factor of 10^3–10^5 in intensity (e.g., Favata et al. 2005; Wolk et al. 2005; Flaccomio et al. 2005; Stassun et al. 2006; Maggio et al. 2007; Caramazza et al. 2007; Arzner et al. 2007; Stelzer et al. 2007; Franciosini et al. 2007).

The decay of PMS X-ray flares on timescales of 10^3–10^5 s has proven particularly amenable to astrophysical modeling. One favored model, developed by Reale et al. (1997) and extensively applied to solar and stellar X-ray flares, considers X-rays produced by thermal plasma at $T \sim 10^7$ K confined in a cylindrical loop and cooled by radiation and conduction, but subject to possible reheating by later magnetic reconnection events. Using such models, inferences can be made concerning magnetic fields responsible for the flare, including loop length and magnetic field strength. For the most powerful PMS flares, inferred loop lengths reach

[1] Department of Astronomy and Astrophysics, 525 Davey Laboratory, Pennsylvania State University, University Park, PA 16802; gkosta@astro.psu.edu.
[2] INAF, Osservatorio Astronomico di Palermo G. S. Vaiana, Piazza del Parlamento 1, I-90134 Palermo, Italy.
[3] SUPA, School of Physics and Astronomy, North Haugh, St. Andrews, Fife KY16 9SS, Scotland, UK.

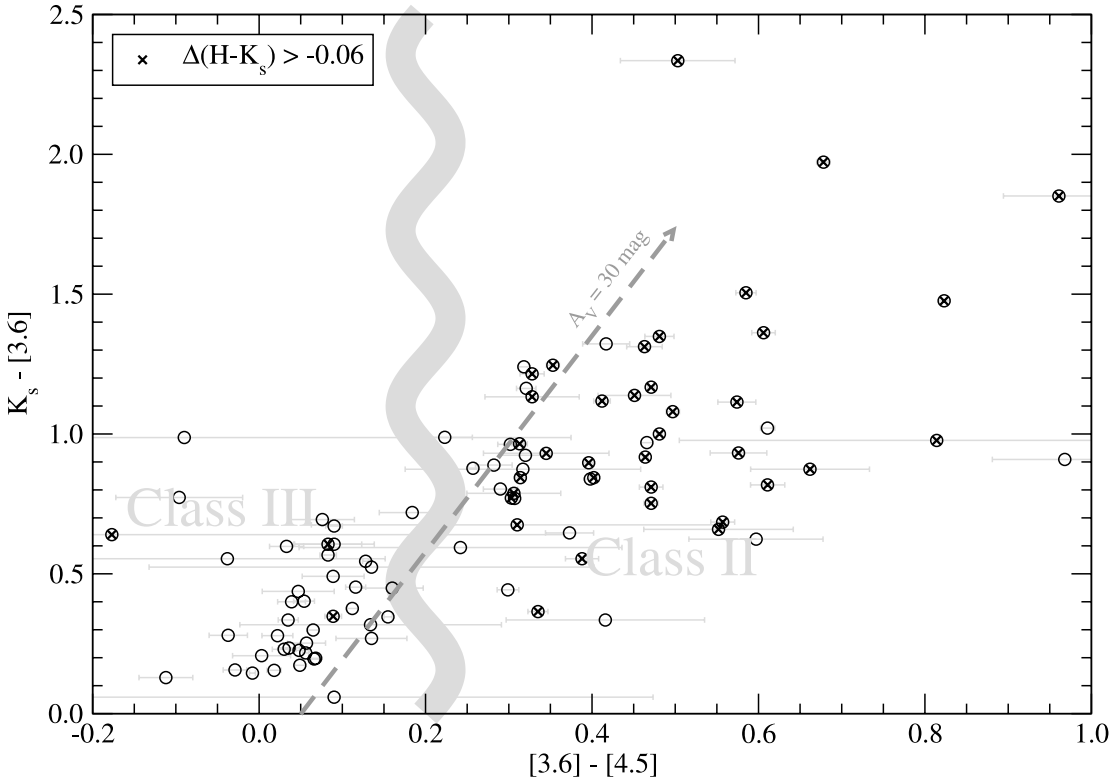

FIG. 1.—Disk indicators $K_s - [3.6]$ vs. $[3.6] - [4.5]$ color-color diagram for 98 COUP sources with available infrared photometry. For 59 sources $\Delta(H - K_s) < -0.06$ mag, indicating no inner disk, while for 39 sources (marked by crosses) $\Delta(H - K_s) > -0.06$ mag, indicating an inner disk. A reddening vector of $A_V \sim 30$ mag is shown by the gray arrow. The wavy gray line roughly discriminates between stars with and without a MIR excess from a circumstellar disk. Typical errors on $K_s - [3.6]$ are 0.02 mag, while errors on $[3.6] - [4.5]$ are shown as gray bars.

4–20 $R_\star$, which is comparable to the expected inner edges of protoplanetary disks (Favata et al. 2005).[4] Thus, X-ray flaring potentially probes the region of star-disk interaction. Links are also emerging between other features of PMS X-ray emission, such as the statistical suppression of flares in accreting systems, the rotational modulation of X-rays, and models of multipolar PMS magnetospheres (Gregory et al. 2006a, 2007).

The present study extends the analysis of powerful flares from COUP made by Favata et al. (2005). They modeled 32 flares using a traditional technique of time-resolved spectroscopy. In Getman et al. (2008, hereafter Paper I) and Getman et al. (2006), we introduce a more sensitive data analysis method based on adaptively smoothed median energies, which permits modeling of 216 COUP flares. This sample is large enough to permit new investigation of possible links between flaring, PMS magnetospheres, and protoplanetary disks. Here, we present observational evidence that X-ray–emitting coronal structures are in fact truncated by inner disks around the Keplerian corotation radius, just as predicted by the PMS theoretical models outlined above. We also report a variety of other results, both positive and negative, linking magnetic flare properties to the presence or absence of disks.

The paper is organized as follows. Preliminary work and recovery of some established results are given in § 2. The main results of our study appear in the following four sections: the absence of strong links between some flare properties and disks (§ 3), clear evidence that PMS magnetospheres do not extend beyond disk inner edges (§ 4), and possible relations between superhot flares, accretion, and non-dipolar magnetic fields (§§ 5 and 6). Discussion follows in § 7. Readers are encouraged to consult Paper I for details on the selection, modeling, and properties of the 216 COUP flares discussed here.

[4] Recall, however, that the vast majority of weaker PMS flares arise in magnetic loops no larger than the star (e.g., Imanishi et al. 2003; Wolk et al. 2005; Franciosini et al. 2007).

2. PRELIMINARY CONSIDERATIONS

2.1. *Disks and Accretion Indicators*

We follow a well-established path in defining the presence of disks and accretion in PMS stars. The K_s-[3.6]-[4.5] color-color diagram in Figure 1 shows 98 sources with available IR photometry (both $\Delta(H - K_s)$ and $[3.6] - [4.5]$; see Table 4 of Paper I). This diagram is known to provide good discrimination between Class I (protostellar), Class II (classical T Tauri), and Class III (weak-lined T Tauri) systems (e.g., Hartmann et al. 2005). The reddening vector of $A_V \sim 30$ mag for a disk-free Vega-like spectrum assuming the reddening law of Mathis (1990) demarcates the locus of Class III objects (on the left) from the Class II and Class I systems (on the right). All 98 COUP objects, except for three with color $[3.6] - [4.5] > 0.5$, have inferred X-ray column densities $\log N_{\rm H} < 22.3$ cm^{-2} (Table 4 of Paper I). For normal interstellar gas-to-dust ratios, this corresponds to a visual absorption of <10–12 mag (Vuong et al. 2003), and thus to a limiting color of $[3.6] - [4.5] < 0.2$ for Class III objects. Several stars to the left of the reddening vector and with $[3.6] - [4.5]$ color in excess of 0.2 may be systems with either higher photometric errors and/or special reddening conditions in their individual star-disk systems. Nevertheless, the rough mid-infrared (MIR) color criterion of $[3.6] - [4.5] = 0.2$ effectively discriminates between Class III and Class II systems, and we use this as our main MIR disk indicator. A few COUP sources with $K_s - [3.6] \sim 2$ may be

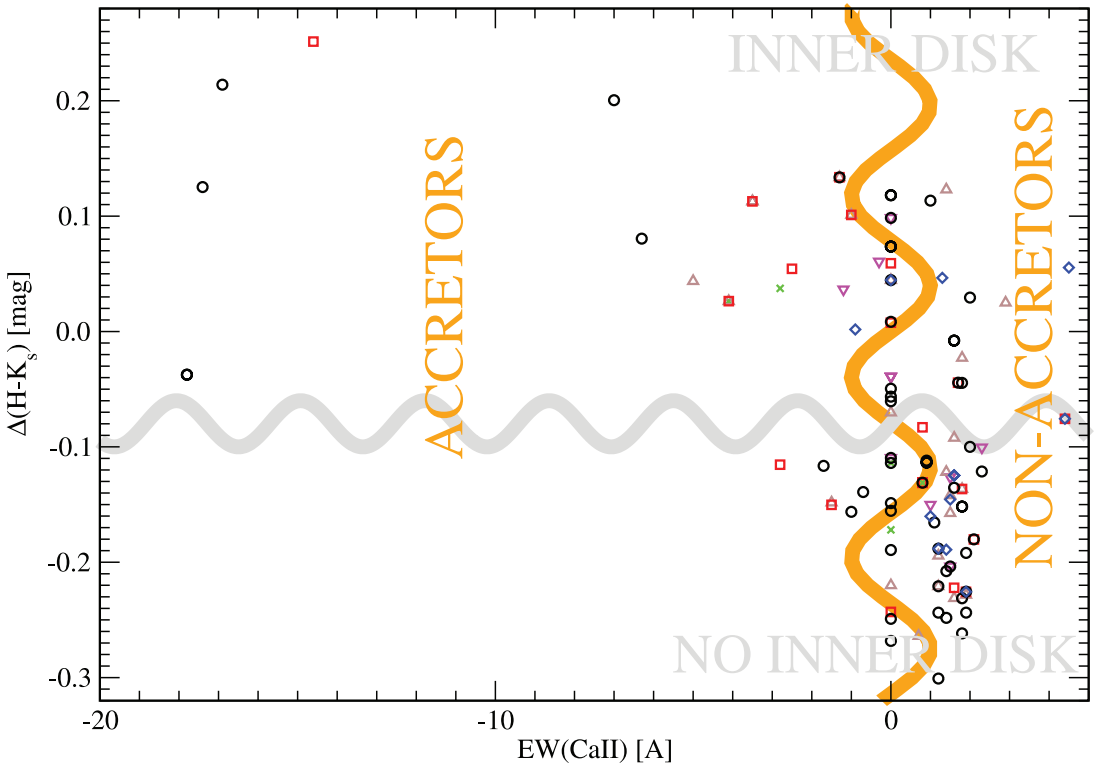

FIG. 2.—Inner-disk indicator $\Delta(H - K_s)$ vs. accretion indicator from the 8542 Å Ca II line for 128 flares on 96 COUP stars with available data. Symbols represent flare morphologies: 57 typical flares (*black circles*), 21 step flares (*red squares*), 12 slow-rise top-flat flares (*blue diamonds*), 23 incomplete flares (*brown triangles*), 5 double flares (*green crosses*), and 10 unclassified flares (*magenta triangles*). The wavy gray line roughly discriminates between stars with and without an inner disk. The wavy orange line very roughly discriminates between stars with and without accretion.

Class I or transitional Class I/II systems. One of them, COUP 570, is classified as a 0/Ib protostellar candidate in Prisinzano et al. (2008).

A $\Delta(H - K_s)$ near-infrared (NIR) excess is an indicator of a heated inner dusty circumstellar disk. It is measured from the reddening vector on the $J - H$ versus $H - K_s$ diagram of COUP sources (e.g., Fig. 5*a* in Favata et al. 2005), adopting photospheric colors associated with PMS stars at age 1 Myr using the models of Siess et al. (2000) and considering a reddening vector applied to 0.1 $M_\odot$ stars. Only four sources in our sample have masses $M < 0.2\ M_\odot$, but 40 have $0.2\ M_\odot < M < 0.4\ M_\odot$. In order to allow better discrimination of inner disks, we can relax the criterion $\Delta(H - K_s) = 0$ mag to a value in the range from -1 to -0.06 mag, which corresponds to reddening vectors in the range of 0.2–0.4 $M_\odot$.

Using this NIR color excess measure, we find that a criterion of $\Delta(H - K_s) = -0.06$ mag is a good discriminator between disk-free and disky stars established with the MIR color criterion of $[3.6] - [4.5] = 0.2$; of sources classified as Class III using this MIR color criterion, 95% are also Class III using our NIR color criterion (Fig. 1). About 17 stars are classified as Class II systems using MIR colors, but as Class III using NIR colors; these systems likely have evolved disks with inner holes.

Discrimination between accreting and nonaccreting objects employs the equivalent width of the IR 8542 Å Ca II line, EW(Ca II), measured from low-resolution spectroscopy by Hillenbrand (1997). In Figure 2, we adopt the classification criterion used by Flaccomio et al. (2003): stars with the line in emission and EW(Ca II) < -1 Å are accretors, while stars with the line in absorption and EW(Ca II) > 1 Å are considered to be nonaccretors. Stars with intermediate values -1 Å $<$ EW(Ca II) < 1 Å have an indeterminate classification. Figure 2 shows that this EW(Ca II) accretion indicator agrees in most cases with the $\Delta(H - K_s)$ NIR inner-disk indicator: inner-disk photometric excess is seen in 15 of the 19 accretors, and no photometric excess is seen in 32 of the 41 nonaccretors. COUP flaring sources with their conservatively chosen EW(Ca II) < -2 Å will henceforth be classified in the text as high accretors.[5]

Recall that photometric and inferred properties (such as age, mass, and rotation) for these COUP stars are tabulated by Getman et al. (2005), while tables in Paper I present various observed and inferred stellar and flare quantities. Tables 1 and 2 of the current paper give general statistical properties of those quantities. They also provide probabilities $P_{\text{K-S}}$ from two-sample univariate Kolmogorov-Smirnov (K-S) tests that compare the distributions of various quantities in disk-free and disky stars. Significant disk effects may be present when $P_{\text{K-S}} \lesssim 0.05$. This is relevant for such quantities as rotational period, Keplerian corotation radius, peak flare plasma temperature, coronal loop size relative to stellar radius, and X-ray coronal extent relative to corotation radius.

2.2. *Disks and Stellar Rotation*

Using our sample of X-ray–bright COUP stars, we confirm the well-established result that Orion Nebula Cluster PMS stars with disks rotate more slowly than those without disks (e.g., Herbst et al. 2002; Rebull et al. 2006). Our rotational periods are obtained from published sources, but our MIR photometry was derived independently from *Spitzer Space Telescope* data, as

[5] The association between accreting stars and MIR-excess stars in our sample is not perfect. Four high accretors located at the outskirts of the *Chandra* field are not part of the MIR disk sample because they lie outside the *Spitzer* IRAC fields from which we obtained MIR photometry. An additional high accretor lies projected against the infrared-bright BN/KL region, which is classified as a disk-free star based on its (possibly erroneous) MIR photometry. See also § 2.3 and Fig. 4.

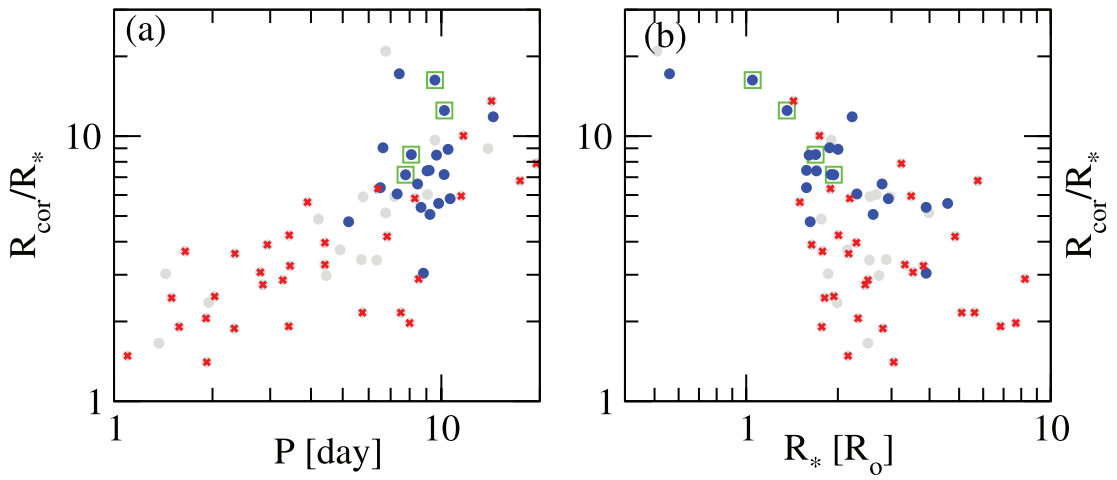

FIG. 3.—Confirmation of PMS disk-rotation relationship. (*a*) Keplerian corotation radius scaled to stellar radius vs. stellar rotational period. (*b*) Keplerian corotation radius scaled to stellar radius vs. stellar radius. Panels present results for all stars with available stellar properties (67 out of 161). Symbols indicate subsamples: stars with MIR-excess disk stars (*blue circles*), without MIR disks (*red crosses*), uncertain disks (*gray circles*), and high-accretion stars with EW(Ca II) < -2 Å (*green boxes*).

described in Paper I, and our classification of disky versus disk-free stars was determined as described above.

This expected result is shown in Figure 3, where stars with MIR disks (*blue circles*) and accretion (*green boxes*) systematically have longer periods and larger corotation radii[6] than disk-free stars (*red circles*). This supports the explanation that slow PMS rotation is due to the loss of stellar angular momentum through magnetic star-disk interaction (see review by Bouvier et al. 2007). Table 1 shows that the rotational periods of our bright X-ray–flaring stars are well separated, with a median of 9.0 days for those with MIR disks compared to 3.5 days for those without MIR disks. The rotational periods of our accreting systems are not distinguishable from those of other stars with MIR disks. It is useful to note that the range of COUP rotational periods of 1–10 days corresponds to a range of corotation radii of 2–10 $R_\star$, with a majority of COUP stellar radii in the range 1.4–3 $R_\odot$ (Fig. 3).

2.3. *Disks and Location in the Cloud*

Figure 4 shows the spatial distribution of our stars with and without MIR disks in the Orion Nebula region. The region is complicated: the rich, optically bright Orion Nebula Cluster has low absorption, and it lies in front of the two OMC 1 molecular cloud cores as well as widely distributed molecular cloud material, where PMS stars are highly absorbed. In the figure, the stars are coded both by their disk properties and by their absorption, as measured from the soft X-ray absorption in their COUP spectra (Getman et al. 2005). The spatial distribution of the COUP stars is further discussed by Feigelson et al. (2005) and Prisinzano et al. (2008).

Bright flaring COUP stars with MIR disks and the highest absorption (Fig. 4*a*, *blue circles*) are largely concentrated around the OMC-1 molecular filament to the north of the Becklin-Neugebauer star-forming region. Those with intermediate absorption have a somewhat broader distribution centered northeast of the OMC cloud cores. The disk-free stars in our sample are generally less absorbed than those with MIR disks, with a dispersed spatial distribution similar to the disky stars with intermediate absorption (Fig. 4*b*). For both samples, stars harboring superhot ($T_{\rm obs,pk} >$ 100 MK; see § 5) flares are localized within the northeastern part of the cloud. The high accretors appear widely dispersed (Fig. 4*c*), but this is a selection effect; only 12 high accretors have observed X-ray net counts above the count threshold of our flare analysis (NC = 4000 counts; see Paper I and footnote 2). The total known population of COUP high accretors has a spatial distribution similar to that of the bright flaring COUP MIR disk stars with intermediate absorption (Fig. 4*d*).

[6] Recall that Keplerian corotation radii for stars with known rotational periods P and masses M are calculated in Paper I as $R_{\rm cor} = (GMP^2/4\pi^2)^{1/3}$.

3. FLARE PROPERTIES AND PROTOPLANETARY DISKS

Paper I presents in detail our analysis of the selected COUP flares and the derivation of flare properties used in the analysis here, i.e., rise and decay timescales, characteristic preflare and peak flare X-ray luminosities, peak flare plasma temperature and emission measure, flare morphology, and the length of the magnetic loop responsible for the flare. These quantities are derived using the astrophysical model of flare decays developed by Reale et al. (1997). This is a single-loop model, and is simplistic in a number of ways (see its limitations in §§ 2.2 and 2.5 of Paper I). However, even in the case of complex flares, it is appropriate to apply the model to a light curve segment if there is an indication for the presence of a single dominant flaring structure (see §§ 2.5 and 2.6 of Paper I).

Adopting the model of Reale et al. (1997), Favata et al. (2005) analyzed the strongest 32 COUP flares using the long-standing flare analysis method of time-resolved spectroscopy (TRS). To extend the flare sample of Favata et al. (2005), Paper I utilizes a more sensitive technique of flare analysis, the "method of adaptively smoothed median energy" (MASME), introduced by Getman et al. (2006). Instead of performing classical TRS with XSPEC over only a few characteristic flare intervals, we employ an adaptively smoothed estimator of the median energy of flare counts and count rate to infer the evolution of plasma temperature and emission measure at dozens of time points along the decay phase of a flare. This is achieved by calibrating the median energies and count rates to temperatures and emission measures through simulations of high signal-to-noise spectra using column densities derived from time-integrated spectral fits (Getman et al. 2005). The method permits modeling of flare spectra on more rapid timescales and with weaker signals than was possible using traditional spectral fitting. Readers are encouraged to consult § 2.2 and Appendices A and B of Paper I on details of the method. The

TABLE 1
SUMMARY OF STELLAR PROPERTIES

Parameter (1)	N (2)	Flag (3)	Min (4)	Max (5)	Median (6)	Mean ± SD (7)	$P_{K\text{-}S}$ (8)
X-Ray–absorbing Column Density (cm^{-2})							
$\log(N_H)$ (all available)	161	s	20.0	22.8	21.6	21.5 ± 0.6	...
$\log(N_{H,NIRdisk})$ (NIR inner disk)	56	s	20.0	22.6	21.7	21.6 ± 0.6	...
$\log(N_{H,noNIRdisk})$ (no NIR inner disk)	84	s	20.0	22.3	21.5	21.4 ± 0.6	0.09
$\log(N_{H,MIRdisk})$ (MIR disk)	62	s	20.0	22.8	21.8	21.7 ± 0.6	...
$\log(N_{H,noMIRdisk})$ (no MIR disk)	50	s	20.0	22.5	21.3	21.3 ± 0.6	0.02
Stellar Mass ($M_\odot$)							
M (all available)	128	s	0.2	5.0	0.7	1.0 ± 0.9	...
$M_{NIRdisk}$ (NIR inner disk)	42	s	0.2	5.0	0.7	1.1 ± 1.1	...
$M_{noNIRdisk}$ (no NIR inner disk)	72	s	0.2	2.3	0.6	1.0 ± 0.8	0.1
$M_{MIRdisk}$ (MIR disk)	44	s	0.2	5.0	0.7	1.1 ± 0.9	...
$M_{noMIRdisk}$ (no MIR disk)	42	s	0.2	2.3	0.6	1.0 ± 0.9	0.4
Stellar Radius (10^{10} cm)							
$R_\star$ (all available)	130	s	4	90	18	20 ± 12	...
$R_{\star,NIRdisk}$ (NIR inner disk)	44	s	5	90	16	19 ± 15	...
$R_{\star,noNIRdisk}$ (no NIR inner disk)	72	s	4	58	18	21 ± 11	0.5
$R_{\star,MIRdisk}$ (MIR disk)	45	s	4	32	14	17 ± 7	...
$R_{\star,noMIRdisk}$ (no MIR disk)	43	s	10	58	17	22 ± 12	0.3
Stellar Rotational Period (days)							
P (all available)	79	s	1.1	19.5	6.5	6.7 ± 3.9	...
$P_{NIRdisk}$ (NIR inner disk)	20	s	1.4	14.4	8.5	7.7 ± 2.8	...
$P_{noNIRdisk}$ (no NIR inner disk)	48	s	1.1	19.5	6.3	6.3 ± 4.2	0.06
$P_{MIRdisk}$ (MIR disk)	24	s	5.2	14.4	9.0	8.8 ± 1.9	...
$P_{noMIRdisk}$ (no MIR disk)	35	s	1.1	19.5	3.5	5.5 ± 4.6	<0.0001
Keplerian Corotation Radius (10^{10} cm)							
R_{cor} (all available)	67	s	22	270	85	90 ± 47	...
$R_{cor,NIRdisk}$ (NIR inner disk)	14	s	39	180	120	107 ± 39	...
$R_{cor,noNIRdisk}$ (no NIR inner disk)	44	s	22	270	84	87 ± 50	0.03
$R_{cor,MIRdisk}$ (MIR disk)	21	s	54	180	98	108 ± 33	...
$R_{cor,noMIRdisk}$ (no MIR disk)	31	s	22	270	76	83 ± 55	0.007
Ratio of Corotation Radius to Stellar Radius							
$R_{cor}/R_\star$ (all available)	67	s	1.4	20.9	5.1	5.7 ± 3.9	...
$(R_{cor}/R_\star)_{NIRdisk}$ (NIR inner disk)	14	s	3.0	16.3	7.4	8.1 ± 3.6	...
$(R_{cor}/R_\star)_{noNIRdisk}$ (no NIR inner disk)	44	s	1.5	20.9	4.2	5.3 ± 4.0	0.01
$(R_{cor}/R_\star)_{MIRdisk}$ (MIR disk)	21	s	3.0	17.2	7.2	8.1 ± 3.6	...
$(R_{cor}/R_\star)_{noMIRdisk}$ (no MIR disk)	31	s	1.4	13.6	3.2	4.0 ± 2.7	<0.0001

NOTES.—Col. (1): Parameter name. Col. (2): Number of flares (Flag=f; see Col. [3]) or sources (Flag=s) in a sample. Col. (3): Indicates whether this is a flare ("f") or source ("s") sample. Cols. (4)–(6): Min, max, and median values for a considered quantity's distribution, respectively. Col. (7): Mean and standard deviation for a considered quantity's distribution. Col. (8): K-S probability for the assumption that distributions of a considered quantity in disky and disk-free stars are drawn from the same underlying distribution.

result is that Paper I characterizes 216 COUP flares, whereas Favata et al. (2005) characterized only 32 such flares.

3.1. *Disks Have No Effect on Flare Morphology*

Paper I describes our qualitative classification of X-ray flares by their light curves during the flare. The four classes are: "typical" flares, with the fast rises and slower decays characteristic of most solar flares; "step" flares, with extra emission during the decay attributable to a reheating or a secondary reconnection event; "double" flares, with two peaks suggestive of two nearly simultaneous reconnection events; and "slow-rise top-flat" (SRTF) flares. The first three classes are commonly seen in solar flares. For example, Figure 11 of Paper I shows solar flares with secondary events during the decay of powerful long-duration events. Such events, scaled up by several orders of magnitude, could be classified as step or double flares in COUP light curves.

The SRTF flares are more unusual, and one may speculate that they may be selectively formed in certain PMS stars. For example, they might be reconnection events associated with sheared star-disk magnetic fields (Montmerle et al. 2000; Isobe et al. 2003) rather than events associated with field lines attached to the star. Flare morphology is coded by different symbols in Figures 2, 6, 7, and 8. We examine here the distribution of flare types along the abscissa measuring the strength of the accretion, NIR inner disk, and MIR disk indicators. No pattern between flare morphology and disk indicators is seen. In particular, SRTF flares

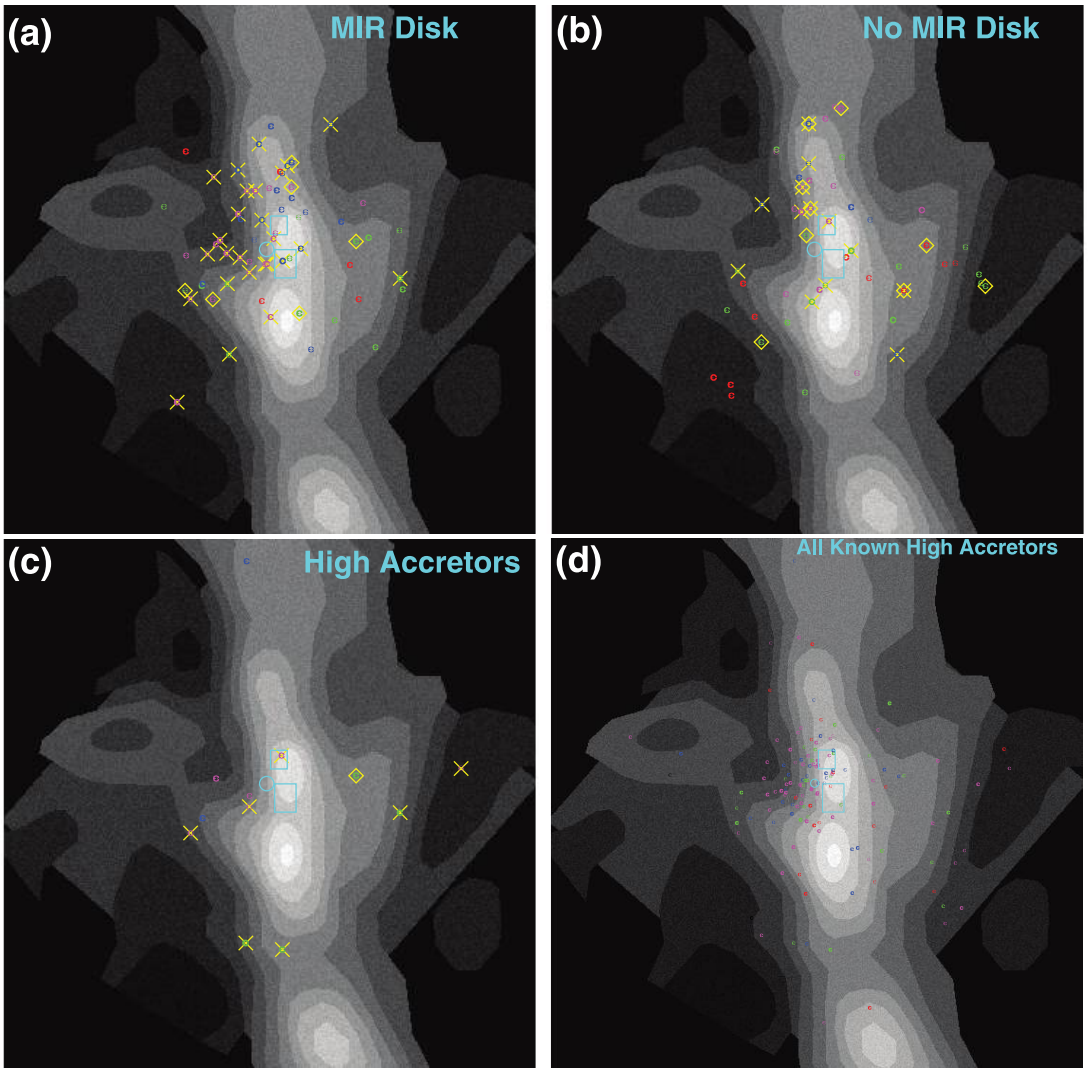

FIG. 4.— Locations of subsamples of X-ray–bright flaring COUP stars plotted on the map of the OMC, derived from the velocity-integrated intensity of ^{13}CO (Bally et al. 1987). Symbols are coded by their X-ray absorption: $\log(N_{\rm H}) < 21$ cm^{-2} (*red*), 21 cm^{-2} $< \log(N_{\rm H}) < 21.5$ cm^{-2} (*green*), 21.5 cm^{-2} $< \log(N_{\rm H}) < 22$ cm^{-2} (*magenta*), and 22 cm^{-2} $< \log(N_{\rm H}) < 22.8$ cm^{-2} (*blue*). Stars with masses $M > 2\,M_{\odot}$ are outlined by yellow diamonds, while stars harboring superhot ($T_{\rm obs,pk} > 100$ MK) flares are labeled by yellow crosses. Two small cyan boxes indicate the BN/KL and OMC-1-S regions (Grosso et al. 2005), and the cyan circle marks θ^1 Ori C at the center of the Orion Nebula Cluster.

are seen in systems both with and without MIR and NIR disks. However, SRTF flares are not seen in high-accretion systems; this can be an indication of a real physical effect (§ 3.2) or simply attributable to the very limited statistics of both accreting and SRTF flare samples.

3.2. *Disks Are Unrelated to Flare Energetics*

We examine here whether any relationships are present between disks and quantities associated with the strength of the X-ray flares, i.e., rise and decay timescales, peak luminosities, and total energies in the X-ray bands.

Figures 5*a* and 5*b* show the distributions of flare rise and decay times stratified by disk and accretion properties. There is a hint that high accretors have systematically shorter flare timescales than the rest of the bright COUP flare sample. The evidence is only suggestive because our sample of high accretors is small (17 flares from 12 sources), and it is only marginally significant when measured by a K-S test ($P = 0.06$ when rise times for high accretors are compared to disk-free systems). Figure 5*c* shows that distributions of flare peak luminosities are indistinguishable for disk-free, MIR disk, and accretion disk systems.

We evaluate the total energies of each of the 216 flares as the difference between the time-integrated flare energy $E_{\rm flare}$ and the energy from the nonflare "characteristic" state $E_{\rm char}$ within the duration of the flare $t_{\rm flare2} - t_{\rm flare1}$. We estimate $E_{\rm flare} \approx L_{\rm X,pk}\,\tau_{\rm decay2}$ and $E_{\rm char} = L_{\rm X,char}(t_{\rm flare2} - t_{\rm flare1})$, where the X-ray luminosity from the characteristic state, $L_{\rm X,char}$, was taken from our TRS analysis (Paper I). Here, $E_{\rm char}$ is systematically lower in flares from high accretors (Fig. 5*d*); this is due to the shorter flare durations (above) and lower $L_{\rm X,char}$ in accreting systems.[7] The latter effect is the well-established suppression of time-integrated X-ray emission in accreting versus nonaccreting PMS systems (Gregory et al. 2007 and references therein). Due to shorter flare timescales, $E_{\rm flare}$ in high accretors shows a somewhat narrower distribution than that of other stars, but the difference is not statistically significant (Fig. 5*e*).

[7] In our flare sample, the effect of lower $L_{\rm X,char}$ in accreting systems is not strong. A K-S test gives only a marginally significant difference ($P_{\rm K\text{-}S} = 0.1$) in $L_{\rm X,char}$ between high accretors and disk-free stars. Median values of $\log L_{\rm X,char}$ are 30.16 erg s^{-1} for disk-free stars, 30.10 erg s^{-1} for MIR disk stars, and 30.10 erg s^{-1} for high accretors.

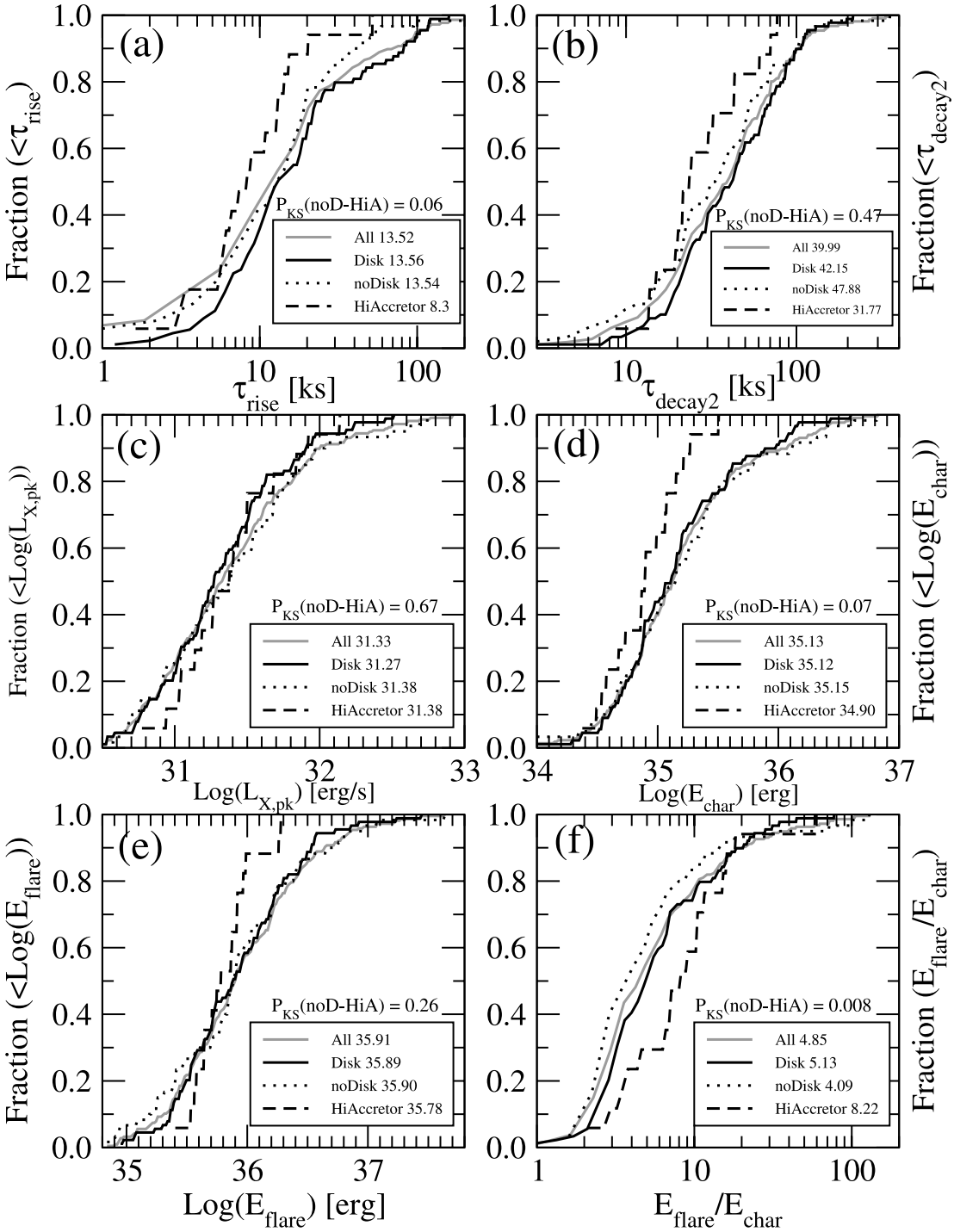

FIG. 5.—(*a*) Cumulative distributions of flare rise timescales. (*b*) Cumulative distributions of flare decay timescales. (*c*) X-ray flare peak luminosity. (*d*) Energy from the "characteristic" state within flare duration time. (*e*) Flare energy. (*f*) Ratio of energies in flare and "characteristic" states. Line types indicate samples: all 216 flares (*solid gray lines*), 89 flares from MIR disk stars (*solid black lines*), 60 disk-free stars (*dotted black lines*), and 17 high accretors (*dashed black lines*). Insets indicate median values, and the K-S test probabilities compare disk-free stars and high accretors.

A more interesting effect is seen in the ratio $E_{\rm flare}/E_{\rm char}$, which is systematically larger in high accretors than in other stars. The median value $E_{\rm flare}/E_{\rm char} \simeq 10$, compared to 5 in disk-free stars ($P_{\rm K\text{-}S} = 0.008$, Fig. 5*f*). In the 840 ks of the COUP observation, a typical single bright flare with a duration of 90 ks (the median of $t_{\rm flare2} - t_{\rm flare1}$ for all 216 flares) may increase the time-integrated source X-ray luminosity 1.5–2 times if $E_{\rm flare}/E_{\rm char} = 5$–10. For a shorter, more typical *Chandra* exposure, a 50 ks bright flare (<22% of flares analyzed here have durations <50 ks) will change the time-integrated source X-ray luminosity by a factor of 3–5.5 if $E_{\rm flare}/E_{\rm char} = 5$–10.

Our major result here is that no difference is found in flare duration, peak luminosity, and total energy between flares occurring in disky and disk-free systems. However, we tentatively find that flares from disky high accretion stars seem to be somewhat shorter, and thus have weaker total X-ray energies, than the rest of the analyzed flares. This tentative finding is supported by two statistically significant findings: (1) that superhot COUP flares

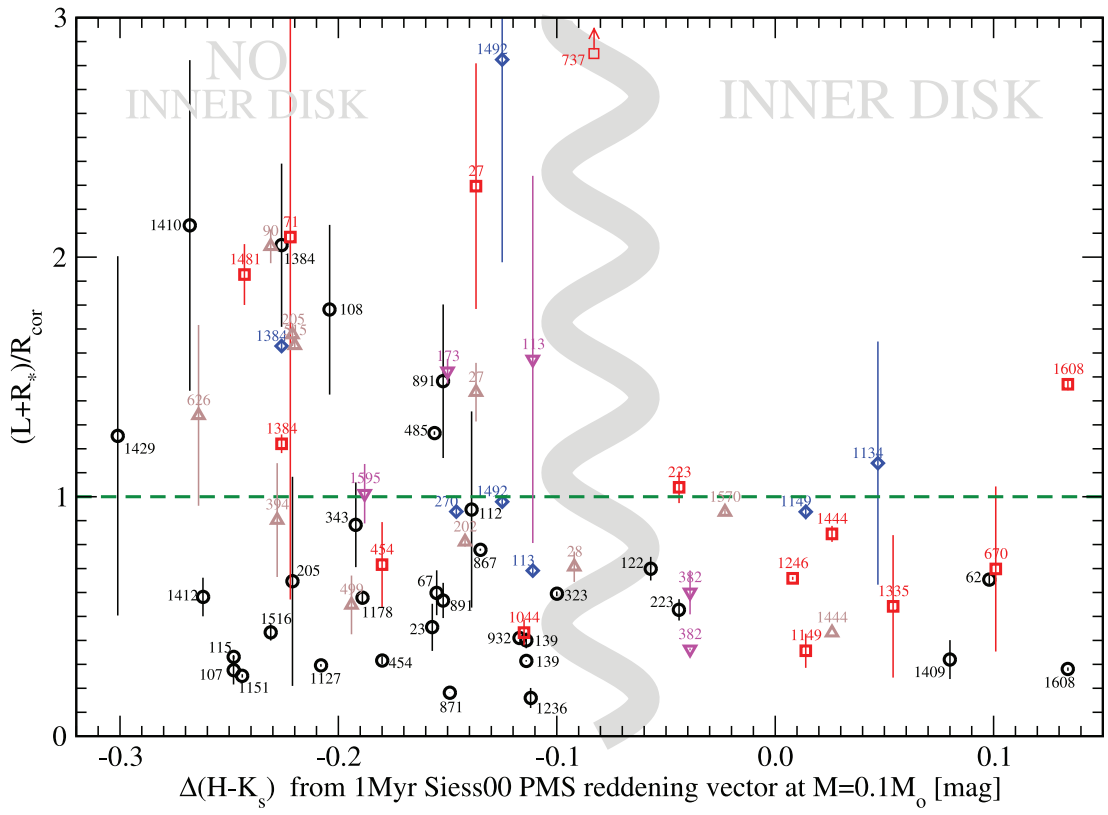

FIG. 6.— Inferred sizes of coronal flaring structures scaled to stellar corotation radii vs. K_s-excess inner-disk indicator. Results are shown for 69 flares from 56 COUP stars with available data. Flares are labeled by corresponding COUP source numbers. Symbols distinguish flare morphologies: 32 typical flares (*black circles*), 14 step flares (*red squares*), 7 slow-rise top-flat flares (*blue diamonds*), 11 incomplete flares (*brown triangles*), and 5 unclassified flares (*magenta triangles*). The wavy gray line roughly discriminates between stars with and without an inner disk. The vertical bars represent boundaries of the ranges of inferred loop size (Paper I), with symbols positioned at the means of those ranges.

are found to be shorter than cooler COUP flares (Paper I), and (2) that superhot flares are preferentially present in accreting systems (§ 5).

4. DISKS MAY TRUNCATE PRE-MAIN-SEQUENCE MAGNETOSPHERES

Figures 6, 7, and 8 compare the flare loop lengths inferred from analysis of the X-ray spectral evolution of the decay phases (Paper I) with our disk and accretion indicators. After careful investigation of various measures of magnetospheric size, we choose to examine the ratio of the coronal extent of the loop as measured from the star center, $L + R_\star$, to the Keplerian corotation radius $R_{\rm cor}$, as determined by the stellar rotation rate. We are thus less interested in the loop size measured in meters than in the relative sizes of the loop to the likely location of the inner edge of the disk. This measure reduces variations associated with star mass, age, and rotation, and focuses on the question of the relationship between PMS disks and magnetospheres.

Figure 6 plots $(L + R_\star)/R_{\rm cor}$ against the NIR $\Delta(H - K_s)$ disk indicator. The vertical lines for each flare do not represent error bars, but are the lower and upper boundaries of the inferred loop size ranges (Paper I), with symbols positioned at the means of those ranges. We find that, except for COUP 1608,[8] coronal structures responsible for flares detected from a dozen sources with NIR inner disks do not exceed $R_{\rm cor}$, while coronal structures responsible for ~40% of flares from 43 sources without NIR inner disks do exceed $R_{\rm cor}$. Some of these flares in disk-free systems arise from loops reaching $\gtrsim 2R_{\rm cor}$. This pattern is present in each morphological flare type (typical, step, double, and slow-rise top-flat), as indicated by different symbols.

The same pattern is seen when $(L + R_\star)/R_{\rm cor}$ is plotted against the MIR disk indicator $[3.6] - [4.5]$ (Fig. 7) and the accretion indicator EW(Ca II) (Fig. 8). Virtually all of the flares whose inferred sizes exceed the host star's corotation radius are disk-free and nonaccreting systems, while disky and accreting flare loops all lie within the corotation radius. The MIR plot adds nine flares from five sources that were not available in the NIR plot; all of these follow the NIR trend. Two outliers, COUP 205 and 485, are those for which the inner part of the disk has likely been cleared of circumstellar material (judging from their NIR colors). Again, the trend is strong and applicable to each morphological flare type. The sample of stars with strong EW(Ca II) emission (indicating active accretion) is smaller than those with infrared photometric excesses, but the trend of smaller loop sizes in accreting systems is still clearly seen.

These three figures provide strong and consistent support for a model in which protoplanetary disks truncate PMS magnetospheres. We do not know of any selection effect that would have produced this pattern in a spurious fashion. The plots in Figure 9 help to elucidate this trend. Here, the symbol colors represent the classification of disky (*blue*) and disk-free (*red*) stars based on MIR colors, and only the mean value of inferred flare loop size is shown. Recall from Figure 3 that, due to the well-established connection between disks and rotation, corotation radii scaled to stellar radii are systematically larger for disky than for disk-free stars (the difference is roughly a factor of 2). This difference in

[8] This outlier is a visual double unresolved by 2MASS, and we suspect that the NIR photometry is unreliable. It lies outside the field of the *Spitzer* IRAC images, so its MIR properties are unavailable.

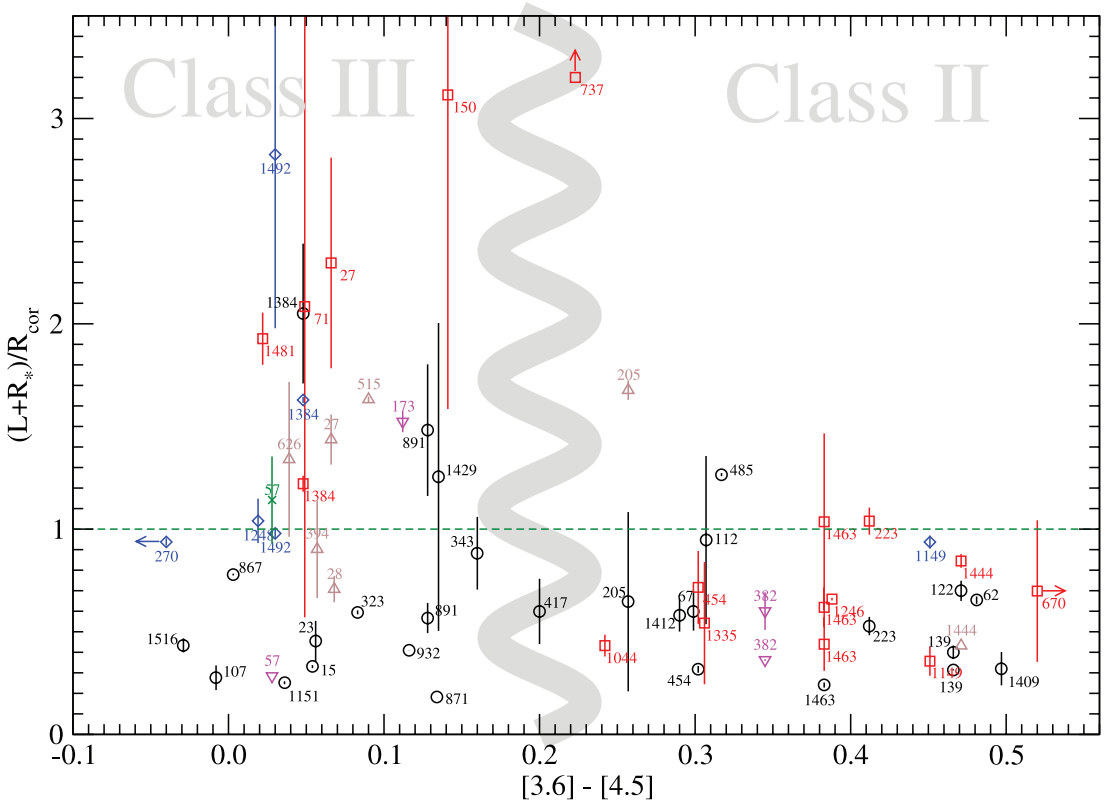

FIG. 7.— Inferred sizes of coronal flaring structures scaled to stellar corotation radii vs. [3.6]−[4.5] MIR disk indicator. Results are shown for 63 flares from 47 COUP stars with available data. Symbols are the same as in Fig. 6.

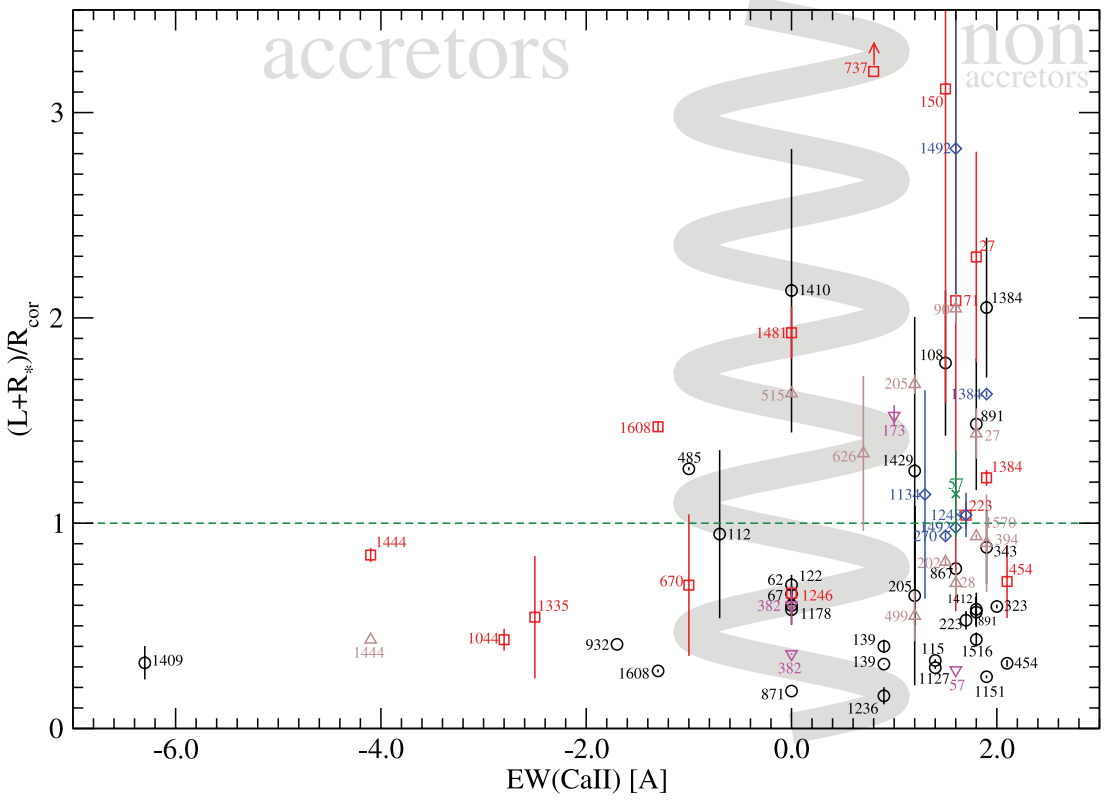

FIG. 8.— Inferred sizes of coronal flaring structures scaled to stellar corotation radii vs. 8542 Å Ca II line accretion indicator. Results are shown for 66 flares from 53 COUP stars with available data. The wavy gray line roughly discriminates between stars with and without accretion. Symbols are the same as in Fig. 6.

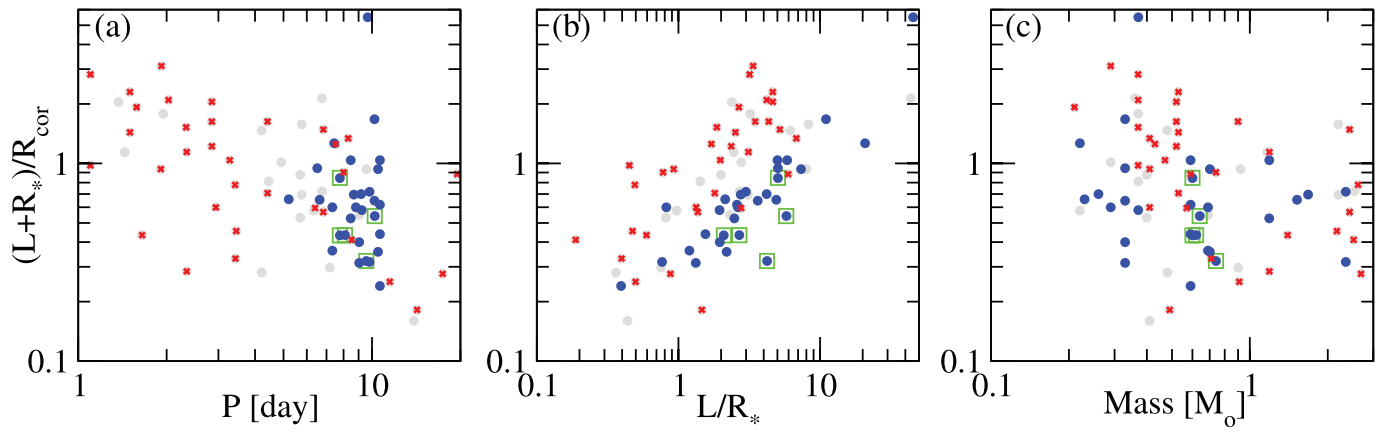

FIG. 9.—Coronal extents of analyzed flaring structures vs. (*a*) stellar rotational period, (*b*) loop size normalized to stellar radius, and (*c*) stellar mass. Symbols are the same as in Fig. 3.

$R_{\rm cor}/R_\star$ is the major contributor to the difference in $(L + R_\star)/R_{\rm cor}$ between the disky and disk-free stars seen in Figures 6–8. If the loop sizes $L/R_\star$ are considered without normalization to the corotation radii, the difference between the two classes becomes marginal.[9]

We thus find that X-ray coronal extents are somewhat similar in disk-free and disky systems, but due to the well-established fact that disk-free stars are faster rotators, the X-ray flares often exceed the corotation radius in these systems. In contrast, X-ray flare loops on disky stars never exceed the corotation radius, although in some cases they reach the corotation radius, which is also the likely truncation radius for the circumstellar disk. The fact that X-ray loops of disky stars come close to but never exceed the corotation radius supports long-standing models of star-disk magnetic interaction at this inner edge involving accretion, outflow ejection, and regulation of the stellar angular momentum. The very large loop sizes seen in all types of PMS stars point to confinement by strong magnetic fields of T Tauri stars, which, particularly in rapidly rotating disk-free systems, are capable of withstanding the effects of centrifugal forces (Jardine & Unruh 1999).

5. SUPERHOT FLARES AND DISKS

Paper I describes the selection of 73 of the 216 COUP flares as "superhot," with peak plasma temperatures $T_{\rm pk} \gtrsim 100$ MK. Similar flares have been occasionally reported in other PMS systems, such as the disk-free binary PMS star system V773 Tau observed with *ASCA* (Tsuboi et al. 1998), two embedded young systems in the NGC 2264 star-forming region (Simon & Dahm 2005), and about half of the COUP flares studied by Favata et al. (2005). However, here we have a sufficiently rich sample to study superhot PMS flares as a class. This is made possible by the large Orion population, the unusually long COUP exposure, and our new highly sensitive flare analysis techniques.

There is some concern that the *Chandra* telescope cannot discern differences in plasma temperatures above ~100 MK due to the rapid decline in mirror reflectivity above ~8 keV. However, we explain in detail in Appendix B of Paper I and in the Appendix below that, when high-signal flares are considered, discriminations between 100 and ≳200 MK peak temperatures, as well as between ≲100 and ≳100 MK, are possible using the median energy as a temperature indicator (our MASME technique described in Paper I). We argue that ≳200 MK superhot peak temperatures were missed by the more traditional time-resolved spectroscopy techniques.

To check on the applicability of the Reale model to unusually large and hot loops, a detailed time-dependent hydrodynamic simulation was applied to a typical superhot flare of COUP source 1343, which has an observed peak flare temperature of a few to several hundred MK and associated coronal flaring structures with derived sizes of $\sim 10^{12}$ cm (§ 4.1 in Favata et al. 2005). The model achieved a peak temperature of ~200 MK and matched both the observed flare spectrum and the light curve. The loop plasma was heated rapidly to ~200 MK on a timescale of 1 hr. This was followed by explosive chromospheric evaporation, with chromospheric plasma reaching the loop apex on a similar timescale of 1 hr, and by the decay phase from the near-equilibrium state governed by conduction and radiation cooling processes on a timescale of a few to several hr.

Table 2 shows that the flare peak temperatures of stars with MIR disks are systematically higher than peak temperatures for stars without MIR disks at high statistical significance ($P_{\rm K\text{-}S} = 0.9\%$). It is not clear why the effect is not seen in *K*-band-excess systems. Figure 10*a* shows that this effect is even more prominent when disk-free stars are compared to high-accretion stars, as based on the Ca II emission line indicator for accretion. Flares from MIR-excess disk stars (Fig. 10, *solid black line*) are hotter on average than those from nondisk stars (*dotted line*), while among flares from disk stars, those from high accretors (*dashed line*) are the hottest. As a consequence, high accretors have the largest fraction of superhot ($T_{\rm obs,\,pk} > 100$ MK) flares, at 53%; stars with MIR disks have 40%, and disk-free stars have 27%. The effect of systematically hotter flares in disk stars and high accretors becomes even more prominent (at a significance level of $P_{\rm K\text{-}S} = 0.02\%$) when only flares from $M < 2\,M_\odot$ stars are considered (Fig. 10*b*). Even when uncertainties on individual values of $T_{\rm obs,\,pk}$ (which can be large for very high temperatures; see Appendix B in Paper I) are taken into account through Monte Carlo simulations, this significance level does not exceed $P_{\rm K\text{-}S} = 1.5\%$.[10]

[9] To avoid observational bias of Class III stars toward higher $R_\star$, we restrict the flare sample to stars with stellar radii in the range $R_\star = 1$–$3\,R_\odot$. This gives the following results. The K-S test shows no statistical difference ($P_{\rm K\text{-}S} = 0.2$) in $L/R_\star$ between Class II and Class III. Median values of $L/R_\star = 3.2$ (2.4) for Class II (III) suggest that $L/R_\star$ for Class II stars is 1.3 times larger than for Class III.

[10] For each of the flare samples (disk-free, disky, and high-accretion), we simulated and compared 10,000 temperature distributions, with individual temperature values randomly drawn from Gaussian distributions with a mean equal to the measured $T_{\rm obs,\,pk}$, and variance as an average error as reported in Appendix B of Paper I. We find that 50%, 68%, and 90% of 10,000 resulting significance levels from the K-S tests between disk-free vs. disky and disk-free vs. high-accretion comparisons do not exceed values of $P_{\rm K\text{-}S} = 0.3\%$, 0.5%, and 1.5%, respectively.

TABLE 2
SUMMARY OF FLARE PROPERTIES

Parameter (1)	N (2)	Flag (3)	Min (4)	Max (5)	Median (6)	Mean ± SD (7)	$P_{K\text{-}S}$ (8)
Peak Flare Luminosity (erg s^{-1})							
$\log(L_{X,pk})$ (all available)	216	f	30.45	32.92	31.33	31.38 ± 0.51	...
$\log(L_{X,pk,NIRdisk})$ (NIR inner disk)	78	f	30.44	32.51	31.35	31.36 ± 0.46	...
$\log(L_{X,pk,noNIRdisk})$ (no NIR inner disk)	106	f	30.53	32.92	31.38	31.41 ± 0.52	0.9
$\log(L_{X,pk,MIRdisk})$ (MIR disk)	89	f	30.49	32.51	31.27	31.32 ± 0.44	...
$\log(L_{X,pk,noMIRdisk})$ (no MIR disk)	60	f	30.57	32.77	31.38	31.40 ± 0.53	0.4
Peak Flare Temperature (MK)							
T_{pk} (all available)	216	f	19	700	63	141 ± 178	...
$T_{pk,NIRdisk}$ (NIR inner disk)	78	f	23	700	73	170 ± 209	...
$T_{pk,noNIRdisk}$ (no NIR inner disk)	106	f	19	700	59	123 ± 153	0.5
$T_{pk,MIRdisk}$ (MIR disk)	89	f	19	700	84	181 ± 209	...
$T_{pk,noMIRdisk}$ (no MIR disk)	60	f	20	600	57	102 ± 114	0.009
Inferred Loop Size (10^{10} cm)							
L (all available)	175	f	0.4	510	43	64 ± 70	...
$L_{NIRdisk}$ (NIR inner disk)	59	f	4	420	43	60 ± 63	...
$L_{noNIRdisk}$ (no NIR inner disk)	89	f	6	510	43	67 ± 71	0.8
$L_{MIRdisk}$ (MIR disk)	68	f	4	510	56	79 ± 86	...
$L_{noMIRdisk}$ (no MIR disk)	54	f	0.4	300	37	54 ± 55	0.12
Ratio of Loop Size to Stellar Radius							
$L/R_\star$ (all available)	147	f	0.03	45	2.4	4.4 ± 7.3	...
$(L/R_\star)_{NIRdisk}$ (NIR inner disk)	48	f	0.14	33	2.5	4.0 ± 5.1	...
$(L/R_\star)_{noNIRdisk}$ (no NIR inner disk)	81	f	0.2	46	2.4	4.6 ± 7.9	0.5
$(L/R_\star)_{MIRdisk}$ (MIR disk)	52	f	0.4	46	3.0	5.9 ± 8.2	...
$(L/R_\star)_{noMIRdisk}$ (no MIR disk)	47	f	0.03	29	1.8	2.9 ± 4.4	0.009
Ratio of Loop Size to Corotation Radius							
L/R_{cor} (all available)	81	f	0.007	5.4	0.51	0.73 ± 0.76	...
$(L/R_{cor})_{NIRdisk}$ (NIR inner disk)	18	f	0.08	1.3	0.51	0.54 ± 0.30	...
$(L/R_{cor})_{noNIRdisk}$ (no NIR inner disk)	51	f	0.05	5.4	0.51	0.82 ± 0.88	0.15
$(L/R_{cor})_{MIRdisk}$ (MIR disk)	30	f	0.07	5.4	0.45	0.66 ± 0.94	...
$(L/R_{cor})_{noMIRdisk}$ (no MIR disk)	33	f	0.007	2.4	0.69	0.78 ± 0.66	0.19
Ratio of Loop Size Plus Stellar Radius to Corotation Radius							
$(L + R_\star)/R_{cor}$ (all available)	81	f	0.16	5.5	0.72	0.98 ± 0.80	...
$[(L + R_\star)/R_{cor}]_{NIRdisk}$ (NIR inner disk)	18	f	0.28	1.5	0.66	0.69 ± 0.32	...
$[(L + R_\star)/R_{cor}]_{noNIRdisk}$ (no NIR inner disk)	51	f	0.16	5.5	0.88	1.11 ± 0.90	0.08
$[(L + R_\star)/R_{cor}]_{MIRdisk}$ (MIR disk)	30	f	0.24	5.49	0.62	0.81 ± 0.94	...
$[(L + R_\star)/R_{cor}]_{noMIRdisk}$ (no MIR disk)	33	f	0.18	3.11	0.98	1.14 ± 0.75	0.01

NOTES.—Col. (1): Parameter name. For loop sizes, data provide a distribution of the mean value of the inferred loop size ranges. Col. (2): Number of flares (Flag = f; see Col. [3]) or sources (Flag = s) in a sample. Col. (3): Indicates whether this is a flare ("f") or source ("s") sample. Cols. (4)–(6): Min, max, and median values for a considered quantity's distribution, respectively. Col. (7): Mean and standard deviation for a considered quantity's distribution. Col. (8): K-S probability for the assumption that distributions of a considered quantity in disky and disk-free stars are drawn from the same underlying distribution.

We thus find strong evidence that superhot flares are preferentially associated with PMS stars undergoing substantial accretion.

Disky stars that possess superhot flares, including accretors, tend to have spectral types late K and M, corresponding to masses $M \lesssim 1$–$2\ M_\odot$, while the majority of disk-free stars with superhot flares are more massive, with spectral types early K through F (Fig. 10*b*, *thin dotted line*). This latter group is not large: for sources with known masses, 66% of the superhot flares are produced by stars with $M < 1\ M_\odot$, while only 15% are produced by stars with $M > 2\ M_\odot$. This can be attributed to the rarity of intermediate-mass stars compared to lower mass stars in the initial mass function.[11] The bottom line seems to be that in low-mass stars ($M < 1\ M_\odot$), the appearance of superhot flares is connected to the presence of active (accreting) disks; however,

[11] Out of 161 COUP stars analyzed here, 83 have known masses of $M < 1\ M_\odot$, and 23 have masses of $M > 2\ M_\odot$. Out of 57 stars producing superhot flares, 27 have known masses of $M < 1\ M_\odot$, and 7 have masses of $M > 2\ M_\odot$. The fraction of low-mass superhot stars (27/83) is comparable to that of higher mass stars (7/23).

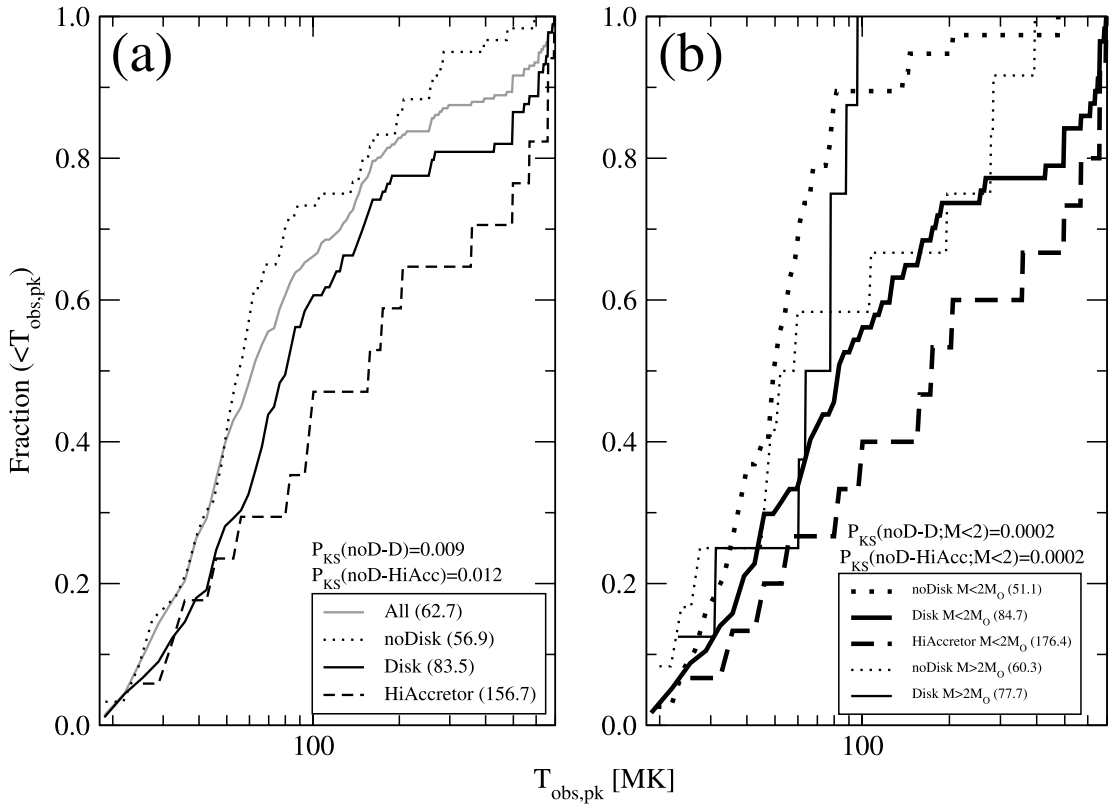

FIG. 10.—(*a*) Cumulative distributions of flare peak temperature for all 216 flares (*solid gray line*), 89 flares from MIR disk stars (*solid black line*), 60 from disk-free stars (*dotted line*), and 17 from high accretors (*dashed line*). (*b*) Mass-stratified cumulative distributions of flare peak temperature for 57 flares from MIR disk stars with $M < 2\,M_{\odot}$ (*thick solid line*), 38 from disk-free stars with $M < 2\,M_{\odot}$ (*thick dotted line*), 15 from high accretors with $M < 2\,M_{\odot}$ (*thick dashed line*), 8 from MIR disk stars with $M > 2\,M_{\odot}$ (*thin solid line*), and 12 from disk-free stars with $M > 2\,M_{\odot}$ (*thin dotted line*). Insets indicate median values, and the K-S test probabilities compare temperature distributions between nondisk stars and disk stars, and between nondisk stars and high accretors.

superhot flares may also arise in massive ($M > 2\,M_{\odot}$) disk-free stars.

6. MAGNETIC FIELD GEOMETRIES

Our analysis can provide indirect access to the geometry and strength of the large-scale magnetic fields responsible for confining the X-ray–emitting plasma during the bright PMS flares studied here. As described in Paper I, the flare decay model gives estimates of the flare plasma peak emission measure ($\mathrm{EM_{pk}}$), coronal loop size (we use here the mean value of the size range, L), and the plasma temperature ($T_{\mathrm{obs,\,pk}}$). If we add an assumption concerning the ratio of the cylindrical loop cross-sectional radius to the loop length β, we can derive the plasma electron density n_e from the emission measure and loop length. The magnetic field confining the plasma can then be estimated assuming pressure equilibrium as

$$B_{\mathrm{eq}} \simeq (8\pi \times 2\, n_e\, k T'_{\mathrm{pk}})^{1/2}, \ \text{where}\ n_e \simeq \left[\mathrm{EM_{pk}}/\left(2\pi\beta^2 L^3\right)\right]^{1/2}. \quad (1)$$

Following past flare models, we adopt a 10:1 cylindrical geometry, $\beta = 0.1$. Here, T'_{pk} is the plasma temperature at the loop apex, which is hotter than the observed X-ray temperature integrated over the entire loop according to $T'_{\mathrm{pk}} = 0.068 \times T^{1.2}_{\mathrm{obs,\,pk}}$, where both temperatures are in units of K (Reale 2002; Favata et al. 2005).

Figure 11 shows the resulting inferred plasma densities (Fig. 11*a*) and magnetic field strengths (Fig. 11*b*) for all (147 of the 162) flares with known loop sizes and stellar radii of their host stars. Plasma density n_e is anticorrelated with the loop size L, as expected from equation (1); the gray line shows the relation $n_e \propto L^{-3/2}$, as expected for constant emission measure and stellar radius. Estimated plasma densities[12] range from 4×10^9 cm^{-3} for very large loop sizes ($L \sim 10R_{\star}$) to 1×10^{12} cm^{-3} for small loop sizes of $L \lesssim 0.2R_{\star}$.

Figure 11*b* plots the equilibrium magnetic field strengths obtained from equation (1) of individual COUP flares against the inferred flare loop lengths. However, the relationship between magnetic field strength and loop length is also a function of field geometry. The simplest geometry often assumed for PMS stars is a dipole:

$$B = \frac{B_{\mathrm{ph}}}{(L/R_{\star} + 1)^3}, \quad (2)$$

where B_{ph} is the photospheric magnetic field, which can be directly measured. Figure 11*b* shows these relations for several photospheric field strengths in the range 1–6 kG, which is consistent with measurements of Zeeman broadening and circular polarization of PMS photospheric lines (Johns-Krull et al. 1999, 2007; Symington et al. 2005; Donati et al. 2007).

[12] We note that the highest loop plasma densities derived here from modeling flare events are comparable to those high densities inferred from high-resolution X-ray spectra that are usually attributed to shocks at the base of accretion streams (e.g., Kastner et al. 2002; Schmitt et al. 2005; Drake et al. 2005; Argiroffi et al. 2007; Güdel & Telleschi 2007; Huenemoerder et al. 2007). This indicates that plasma density alone may not be a reliable discriminant between flare and accretional X-rays.

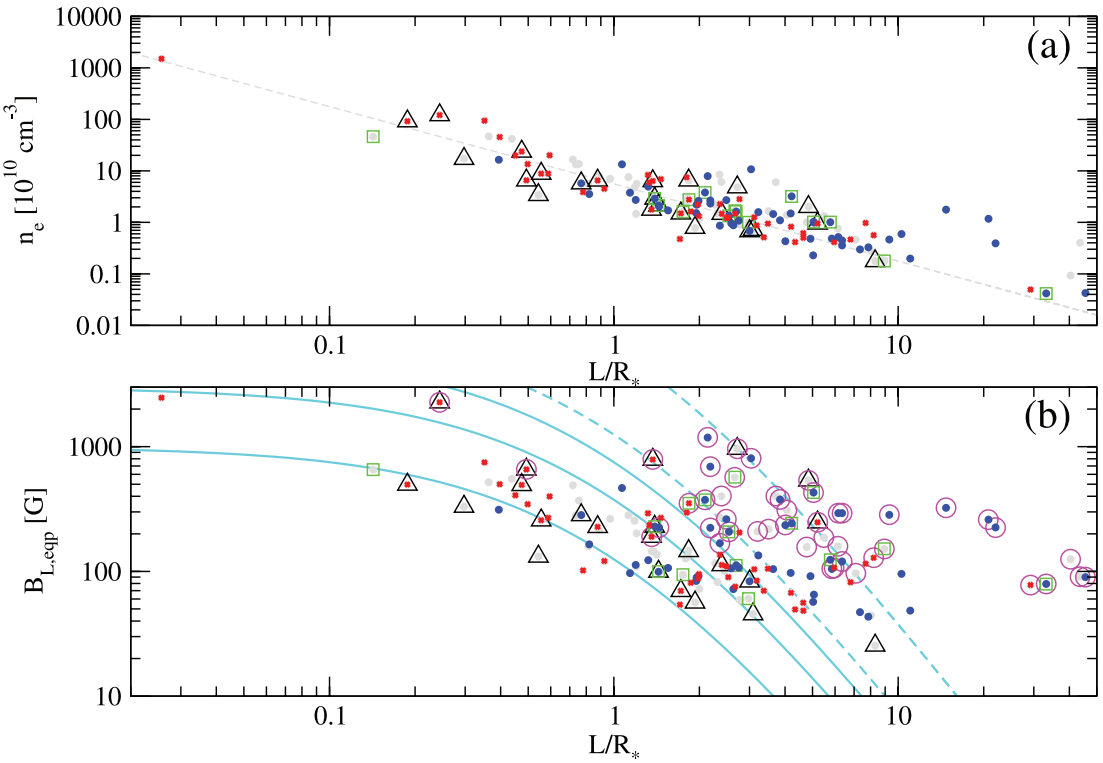

FIG. 11.—(*a*) Estimated plasma density at flare peak and (*b*) magnetic field from pressure equipartition plotted against inferred loop sizes scaled to stellar radii. Symbols discriminate subsamples: MIR disk stars (*blue circles*), no MIR disk stars (*red crosses*), uncertain MIR disk stars (*gray circles*), high-accretion stars with EW(Ca II) < -2 Å (*green squares*), masses $M > 2\,M_\odot$ (*black triangles*), and superhot flares with $T_{\rm obs,pk} > 100$ MK (*magenta circles in panel b*). In panel *a*, the dashed gray line indicates $n_e \propto L^{-3/2}$. In panel *b*, the cyan curves represent loci of photospheric dipolar magnetic fields $B_{\rm ph} = (1, 3, 6)$ kG (*solid lines*) and (10, 50) kG (*dashed lines*).

Figure 11*b* shows that for most of the flares, the magnetic fields estimated assuming pressure equilibrium are consistent with the assumption of dipole geometry, with photospheric magnetic strengths comparable to the observed values of 1–6 kG. These include all types of systems: disk-free stars (*red circles*), MIR disk stars (*blue circles*), active accretors (*green boxes*), and higher mass stars (*black triangles*). Thus, the majority of the flares from our flare sample are associated with the extended, dipole-like loops, and, as already discussed in Paper I, are different from the previously reported smaller stellar flares, which take place in the complex surface field regions likely making up the "characteristic" level of X-ray emission.

However, about 40 flares have inferred field strengths too strong for their inferred loop lengths and/or have loop lengths too long for any realistic dipole model. Nearly all of these discrepant flares have superhot peak temperatures (Fig. 11*b*, *magenta circles*). If a dipolar topology and pressure equilibrium holds, the implied surface magnetic field is tens of kG, which is far above reasonable values.

This discrepancy cannot be fully explained by uncertainties in inferred peak flare temperatures. Both Appendix B of Paper I and the Appendix below provide detailed evidence that the existence of superhot peak temperatures with $T_{\rm obs,pk} > 100$ MK, and often >200 MK, is reliable. The uncertainties of these superhot temperatures shown in Figure 15 of Paper I propagate into loop size uncertainties of 40% and magnetic strength uncertainties of 10%. The confidence regions of most superhot flares in Figure 11*b* thus lie above the locus of dipolar fields with photospheric strengths of $B_{\rm ph} \sim 10$ kG.

As discussed in § 5, superhot flares appear to be associated with the presence of a disk and high accretion. We thus emerge with evidence for anomalous magnetic fields associated with accreting PMS stars. Superhot flares typically arise in large coronal loops $L/R_\star \gtrsim 2$, but still inside the corotation radius. In § 7.1, we speculate that such anomalous fields may result from the distortion of magnetic topologies or the thickening of magnetic loops by the process of accretion.

7. DISCUSSION

7.1. *Does Flaring Occur in Star-Disk Magnetic Fields?*

The first result we encounter in this study is negative: disks appear to have no effects on flare morphology, timescales, or energetics (§§ 3.1–3.2). This is not a trivial finding; there is no reason to believe that flares arising in field lines attached to the inner rim of the circumstellar disk would have the same power, plasma properties, and temporal evolution as flares from magnetic loops anchored in the stellar surface. Reconnection in star-disk loops can occur in several ways: by magnetic interactions between star and disk fields near the corotation radius (Hayashi et al. 1996), by stochastic fluctuations in the accretion rate near the corotation radius (Shu et al. 1997), or by twisting of star-disk loops from stars slightly out of corotation with their disks (Birk et al. 2000; Montmerle et al. 2000). Isobe et al. (2003) calculated the hydrodynamical response of cool plasma to a sudden reconnection event in the middle of a 1×10^{12} cm star-disk loop. They found that the shock reaches both the stellar and disk surfaces in 1–2 hr, with bulk plasma motions sometimes exceeding 1000 km s^{-1}. Temperatures quickly reach 50–100 MK, but the rise in emission measure sometimes appears slower and less regular than in typical solar-type flares. These might be classified as SRTF or double flares. Remarkably, Isobe et al. find that the entirety of the inner-disk gas can be vaporized by powerful reconnection events.

Thus, although SRTF and double flares conceivably could arise exclusively in star-disk loops, our results indicate that this is not the case. Instead, we find that all flare morphological types occur equally in both disk-free and disky systems, with similar luminosity and duration distributions. We therefore conclude that all flare types likely arise in traditional solar-type magnetic loops, where both footpoints are rooted in the stellar surface. This idea is supported by the similarity of COUP flaring statistics and plasma elemental abundance anomalies to those seen in older magnetically active stars (Wolk et al. 2005; Maggio et al. 2007; Stelzer et al. 2007). Figure 11 in Paper I shows that step and double flares are commonly seen in the contemporary Sun, often because of a triggered reconnection or a reheating event. Slow-rise top-flat flares may be similar to other flares, with reconnection sequentially progressing along multiple magnetic arcades. Thus, all types of COUP flares may arise from solar-type magnetic morphologies.

However, the solar-type flare analogy to powerful, long-lasting COUP flares faces a challenge. Jardine & Unruh (1999) have raised the issue that very large magnetic loops anchored to rapidly rotating stars may be destroyed when the centrifugal force of their confined plasma exceeds the weakening magnetic tension in the outer part of the loop. Favata et al. (2005) considered this instability to be a strong argument in favor of attaching long loops to the circumstellar disks. We tentatively conclude from our findings that, while this centrifugal force might break some magnetic loops, others survive to produce the observed powerful flares in disk-free, rapidly rotating COUP stars.

There is one flare parameter that is linked to the presence of a disk: flares on Class II and high-accretion stars have systematically hotter peak flare temperatures (§ 5 and Table 2). This may point to star-disk reconnection as modeled by Isobe et al. (2003), where temperatures of 100 MK are easily achieved. Additional calculations should be made to establish the conditions where peak temperatures of 200 MK or more occur. However, it is also possible that these higher temperatures are a by-product of systematically higher surface magnetic fields in Class II systems, which would be capable of confining hotter plasmas. Younger systems might have stronger fields due to vigorous dynamo precesses (Browning 2008), a primordial field component (Johns-Krull 2007), and/or accretional processes (Bessolaz et al. 2008). Hotter peak temperatures could be a by-product of the magnetospheric compression by disks discussed in § 7.2 or of atypical coronal loop geometries with larger aspect ratios than typical of solar coronal loops ($\beta \gg 0.1$). Rare examples of such "thick" stellar coronal loops are reported in the literature; for example, the AB Dor 29 flare of 1997 November has an estimated $\beta \sim 1$ (Maggio et al. 2000; Reale 2007). We conclude that the correlation between peak flare temperature and disks is an interesting new result, but does not appear to have a unique explanation, and does not clarify whether or not reconnection occurs in star-disk field lines.

7.2. *Magnetospheric Truncation by a Disk*

Our second observational result is positive: the COUP flares provide the first direct evidence that the magnetic loops of powerful X-ray PMS flares can exceed the stellar corotation radius in disk-free stars, but do not exceed the corotation radius in disky stars (Figs. 6–8). This finding is presented visually in Figure 12, which shows with realistic relative scaling the largest inferred X-ray coronal extents for Class II and Class III stars. The high-order multipolar component of the magnetic field is expected to dominate at the stellar surface, but to fall off rapidly with height, leaving the dipolar component dominant at distances above a couple of stellar radii (Fig. 15 in Donati et al. 2007; Donati et al. 2008). Figure 12 also shows schematically a compression and distortion of magnetic field lines by the accretion disk. More realistic field configurations with both accreting field lines and coronal loops are calculated by Jardine et al. (2006) and Long et al. (2007).

For a T Tauri star with radius of $\sim 2\ R_\odot$ and a mass of $\sim 0.5\ M_\odot$, the typical large flaring magnetic loops are roughly the same as for the disk classes with $L/R_\star \sim 5$. However, due to the strong rotational acceleration experienced after the disks are gone, the corotation radii shrink so that loops that were formerly $(L + R_\star)/R_{\rm cor} \lesssim 1$ during their disky phase are often $1 \lesssim (L + R_\star)/R_{\rm cor} \lesssim 2$ during their disk-free phase. Table 1 shows that, as stars evolved from Class II to Class III phases, the average corotation radii decreased from $R_{\rm cor} \sim 7R_\star$ to $\sim 3R_\star$ due to a shortening of the average rotation periods from $P \sim 9$ days to ~ 3 days.

There are three independent supporting lines of evidence suggesting that long-loop structures can be present in magnetically active stars when disks are not present.

1. Even the relatively inactive Sun has helmet-like X-ray streamers that reach up to $\gtrsim 0.5\ R_\odot$ above the photosphere. These occur in the subclass of the solar long-decay events (LDEs). The analogies between solar LDEs and COUP bright X-ray flares are discussed in Paper I and in § 7.3 below.
2. Mullan et al. (2006) have carefully compared the loop sizes inferred from 106 flares studied with the *EUVE* satellite from 33 magnetically active main-sequence stars, including members of RS CVn binaries and dMe stars. They find that stars with $B - V < 1.4$ (hotter than M0) generally have loop lengths $L/R_\star < 0.5$, while stars with $B - V > 1.4$ (cooler than M0) often exhibit loop lengths $L/R_\star \sim 1.0$–1.5.
3. Radio VLBI studies have shown that magnetospheres likely extend several stellar radii in very active stars, and are filled with transrelativistic electrons emitting gyrosynchrotron radiation. This is indicated by VLBI imaging of the RS CVn binary systems UX Ari HR 1099 and HR 5110, and the dMe stars YY Gem and UV Cet (Lang 1994; Alef et al. 1997; Benz et al. 1998; Franciosini et al. 1999; Ransom et al. 2002, 2003). While none of these systems showed loops larger than ~ 2 times the photospheric radius, recent VLBI mapping of the nearby disk-free PMS binary system V773 Tau reveals radio structures extraordinarily far from the component stars. Their elongated magnetospheres resemble huge solar helmet streamers extending $\simeq 20R_\star$, yet they are still anchored to the stellar surface (Massi et al. 2008).

As PMS stars lie at the extreme high-luminosity end of the 10^{10} range of correlated X-ray and radio luminosities (the Benz-Güdel relation; see Fig. 6 in Güdel 2002), it is reasonable that they also have the largest flare loop sizes. While the typical large coronal structures we find from COUP X-ray flares are ~ 5 times the stellar radius, even larger structures are found in some cases. These magnetic structures must extend significantly beyond the corotation surface, implying that the loop magnetic fields are, at least temporarily, capable of withstanding both the thermal pressure of the confined hot gas and the effect of centrifugal forces (Jardine & Unruh 1999).

Our finding that the coronal structures in more slowly rotating Class II stars do not exceed their corotation surface agrees well with the T Tauri coronal models of Jardine et al. (2006). Combining average COUP levels of X-ray emission with optical-band measurements of multipolar surface magnetic fields and magnetic circumstellar disks, they calculate self-consistent three-dimensional

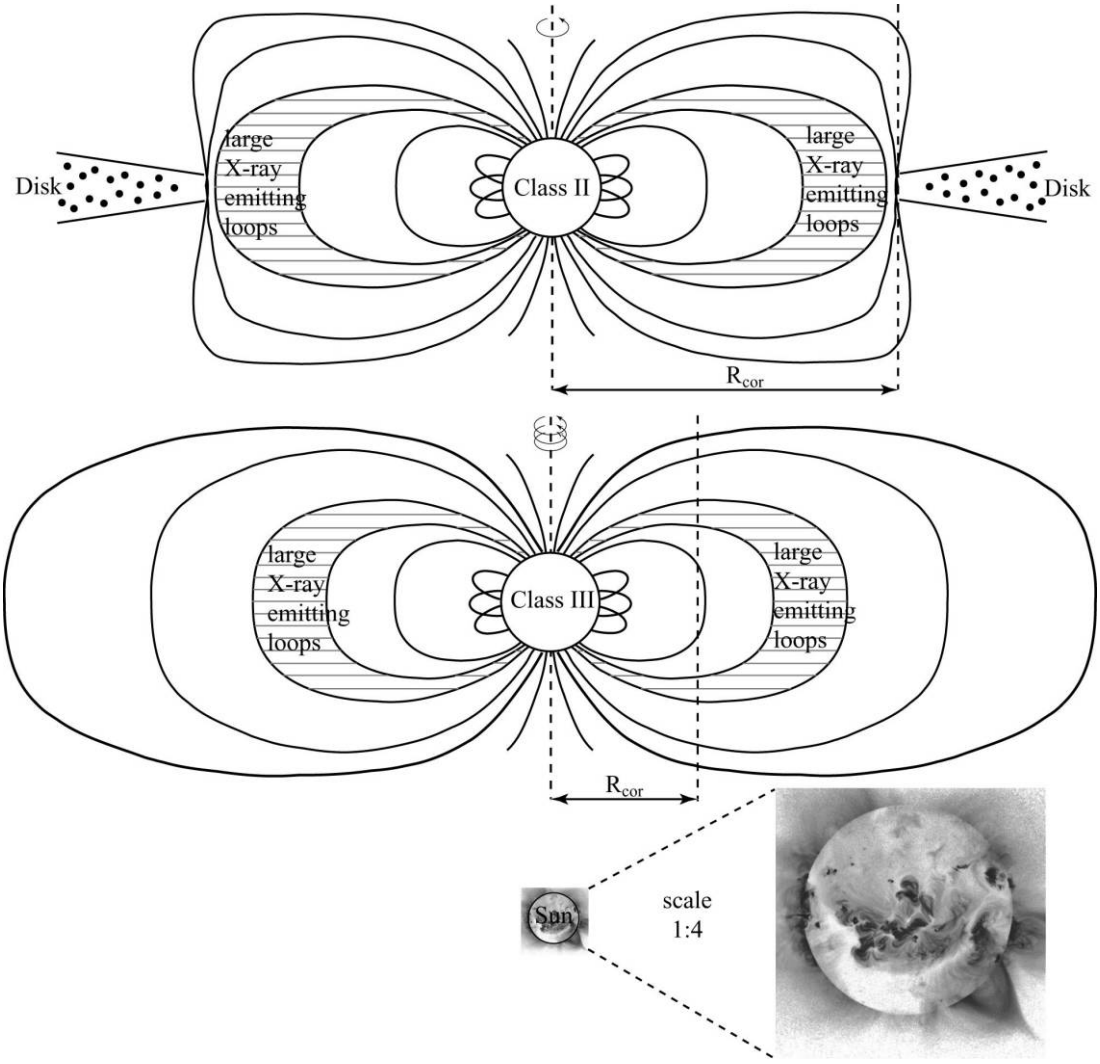

FIG. 12.—Typical sizes of the largest X-ray–emitting magnetic structures, assuming a dipolar geometry (*hatched area*) for Class II and Class III T Tauri stars. Relative sizes are shown to scale for typical stars. The inset shows the X-ray image of the Sun, both to scale and (for clarity) expanded by a factor of 4, with large helmet-like X-ray streamers (1992 January 24 flare; *Yohkoh* SXT).

force-free field configurations. Their model emerges with a complicated combination of closed loops confining X-ray–emitting plasma and open field lines available for accreting cool disk material or releasing a high-velocity wind (see also Lovelace et al. 1995; Long et al. 2007). In the model of Jardine et al. (2006), X-ray coronal extents for disk-free PMS stars reach $(1.5–2.5)R_{cor}$, precisely the range we find in the current work (Figs. 6–8). The centrifugal stripping of the coronal outer parts proposed for rapidly rotating main-sequence stars (such as VXR 45, with a rotation period around 0.2 days; Jardine 2004), is apparently unimportant for relatively slowly rotating T Tauri stars.

We thus find that, while flare properties are mostly similar in Class II and Class III stars (§ 7.1), some differences are found. X-ray coronal structures on Class II stars are, on average, somewhat larger and more likely to produce superhot flares. This suggests that the magnetic fields on accreting Class II stars may have distorted magnetic topologies, as Jardine et al. (2006) predict. We discuss this further in § 7.4.

7.3. *Comparison with Solar Long-Decay Events*

It is reasonable to propose that the majority of the bright, long, X-ray flares detected from Orion T Tauri stars are enhanced analogs of eruptive solar flare events classified as LDEs (Kahler 1977). The *Skylab*, *SMM*, and *Yohkoh* space observatories show that these flares produce X-ray–emitting arches and streamers with altitudes reaching up to several $\times 10^{10}$ cm ($\gtrsim 0.2\ R_\odot$; Švestka et al. 1995, 1997; Fárnik et al. 1996). The X-ray streamers of 1992 January 24, which reached up to $L \gtrsim 0.5\ R_\odot$ in altitude (Hiei 1994, 1997), are representative of magnetic structures emerging from solar LDEs (see inset in Fig. 12). The X-ray light curves of LDE flares last from a few hours to 1 day, a duration similar to that of the COUP flares studied here (see Fig. 14 in Paper I for two examples).

The origin of giant solar X-ray–emitting arches and streamers is not well understood. The most widely accepted model is that the impulsive flare near the solar surface ($L \lesssim 10^{-2}\ R_\odot$) blows open the overlying large-scale magnetic field with subsequent reconnection of magnetic lines through a vertical current sheet. This model was developed over many years (e.g., Sturrock 1966; Kopp & Pneuman 1976; Forbes & Acton 1996), and is reviewed by Priest & Forbes (2002). Peak observed temperatures in giant solar arches and streamers are typically of several to $\gtrsim$10 MK, with a wide range of plasma densities. For example, the 1992 January 24 event showed a relatively low density $\lesssim 10^8$ cm^{-3}, while the 1993

March 15 event showed densities $\gtrsim 10^{10}$ cm^{-3} (Getman & Livshitz 1999, 2000). Recall, however, that the peak luminosities and total energies of these solar flares are far below those we are studying in COUP stars, roughly $E \sim 10^{30}$–10^{31} ergs versus $E \sim 10^{35}$–10^{37} ergs in the X-ray band integrated over the flare.

Confining a solar flare plasma with $n_e \lesssim 10^8$ cm^{-3} and peak temperatures $T \lesssim 10$ MK requires a local field strength exceeding 1 G. In the solar corona, the dipole component appears to become dominant at 2.5 $R_\odot$ (Luhmann et al. 1998), and the Sun's magnetic dipole field, which is only ~1 G at the surface, likely falls ≲0.1 G at this distance. Small-scale multipolar fields in active regions have surface strengths around 1000 G, but these quickly decay at large distances. Thus, the solar fields are too weak to confine X-ray–emitting plasma at distances comparable to or exceeding the solar radius. The large-scale magnetic field of T Tauri stars must thus be far stronger than in the Sun, as argued by Jardine et al. (2006) and others (§§ 7.2, 7.4), and can sustain giant X-ray arches and streamers with sizes $L/R_\star \sim 1$–10. The recent reported discovery that two solar-type radio-flaring streamers in the young binary system V773 Tau A reached altitudes of $>20R_\star$ but were apparently anchored at the surface of their host star (Massi et al. 2008) further strengthens the idea of strong, large-scale magnetic fields and giant, X-ray–emitting flaring structures anchored at the stellar surface of T Tauri stars.

We recall in this context our tentative finding (limited by small samples to a low statistical significance) that flares in accreting systems are systematically shorter than in other systems (§ 3.2). If this is true, it might be that high accretion may prevent very long lasting flares. In order to have relatively long-lasting flare events, magnetic stresses must build up over an extended time, storing magnetic energy accumulated from shearing and twisting of magnetic field lines. A similar process occurs in two-ribbon solar flares (Priest & Forbes 2002), although with much lower total energies. The magnetic field must be stable in order to store large stresses. It is possible that the process of accretion destabilizes the field, preventing the accumulation of magnetic stresses and forcing shorter flares.

We thus suggest that systematically shorter flare durations due to disrupted magnetic field configurations may be responsible for the well-established reduction in time-integrated X-ray luminosities of accreting PMS stars compared to nonaccreting stars. This interpretation is different from past explanations. Preibisch et al. (2005) suggested that X-ray emission from accretors is suppressed because it cannot arise in magnetic field lines that are mass loaded with disk material. Jardine et al. (2006) argued that the outer magnetosphere of accretors is stripped by interaction with the disk. Gregory et al. (2007) proposed that soft X-ray emission is attenuated by dense material in accretion columns. The true cause of the reduced X-ray emission of Class II systems is thus still uncertain.

7.4. *Anomalous Superhot Flares in Accreting Stars*

We described in § 5 and in Paper I a significant subset of COUP flares exhibiting peak temperatures exceeding 100 MK, with some apparently exceeding 200 MK. These temperatures are hotter than any solar flare plasma, and hotter than nearly all reported stellar flares. The only comparable event we have identified is the $T > 180$ MK plasma temperature in the 2005 December 16 flare in the RS CVn system II Peg using the hard X-ray detector (designed for gamma-ray burst discovery) on board the *Swift* satellite (Osten et al. 2007). While the calibration of *Chandra* ACIS median energies to plasma temperatures above ~100 MK is not precise, we argue in Appendix B of Paper I and the Appendix below that these events are indeed hotter than other flares in the sample.

While the superhot flare phenomenon may have more than one cause, the clearest relation is to active accretion in lower mass PMS stars. These are systems where the stellar radius is small, and the stellar magnetosphere appears truncated by the inner disk at the corotation radius (§ 7.2). We show in § 6 that these temperatures are too hot to be explained by standard dipolar fields rooted in the stellar surface. We speculate in § 7.1 that these conditions lead to a compression and intensification of field strength in the outer regions of the loop, where the observed X-ray emission originates. This might lead to more violent reconnection and successful confinement of higher pressure plasmas. This interpretation qualitatively agrees with recent MHD computations of accretion funnels through PMS magnetospheres, where distortion of initially dipolar field lines is predicted (Jardine et al. 2006; Bessolaz et al. 2008; Romanova et al. 2008). Other explanations, such as reconnection in disk-derived fields (e.g., Hayashi et al. 1996), seem less attractive given the similarity of superhot and normal-temperature flares in other respects (e.g., flare morphology and energetics).

8. CONCLUSIONS

We examine here empirical relationships between magnetic reconnection flares, protoplanetary disks, and accretion. The current work provides detailed flare modeling of a much larger data set than previously available: we consider 216 bright X-ray flares from 161 PMS stars observed during the 13 day COUP exposure of the Orion Nebula. Our sample is larger because, as described in Paper I, we use data analysis techniques that permit modeling of fainter flares than feasible with traditional parametric modeling of variable *Chandra* ACIS spectra. We thus have an opportunity to uncover more subtle relationships between flaring, disks, and accretion than was previously possible. The main results of our study are as follows.

1. Perhaps with the exception of the *Chandra* study of NGC 2264, where classical T Tauri stars are seen to be more variable than weak T Tauri stars (Flaccomio et al. 2006), past studies using smaller samples have not found differences in flare statistics or properties as a function of PMS evolutionary state or mass. Accreting Class II systems appeared to flare in the same way as nonaccreting Class III systems (e.g., Stelzer et al. 2000, 2007; Wolk et al. 2005; Favata et al. 2005). We confirm here that Class II and Class III systems produce X-ray flares with indistinguishable morphologies. Typical fast-rise slow-decay flares, composite step and double flares, and the unusual slow-rise top-flat flares are present in both classes. We have no clear evidence for distinctive flare types emerging from star-disk magnetic field lines. Accretion variations producing optical band variations are not associated with X-ray flares (Stassun et al. 2006). Accretion and magnetic flaring thus appear to be unrelated, even though the theory of PMS accretion involves magnetic truncation of disks and magnetic funneling of disk material onto the stellar surface. The COUP PMS flares are consistent with solar-type magnetic structures with both footpoints anchored in the stellar surface. Many may represent analogues of a much less powerful class of solar flares known as long-duration events, which produce giant coronal arches and X-ray streamers.

2. A distinct difference is found in the distribution of loop sizes. We find that X-ray coronal extents in rapidly rotating Class III stars sometimes exceed the Keplerian corotation radius, whereas X-ray magnetospheres in Class II stars appear to be truncated at

the inner edge of accreting protoplanetary disks. This directly supports theoretical models of magnetically mediated accretion, magnetic star-disk rotational coupling, and disk confinement of PMS magnetospheres.

3. A related but statistically less secure result is that flares from high-accretion Class II stars have somewhat shorter durations and weaker total X-ray energies than Class III flares. This might reflect the destabilization of magnetic arcades in accreting systems, and could account for the reduction of time-averaged X-ray luminosities in Class II compared to Class III populations noted in previous studies.

4. A subclass of superhot flares with peak plasma temperatures greater than 100 MK is noted for the first time. These are inconsistent with formation in normal dipolar magnetic loops attached to the stellar surface, and appear preferentially in accreting Class II systems. They may reflect compression and distortion of the large-scale magnetospheric topology by star-disk magnetic interactions, as predicted by recent theoretical calculations.

We thank the anonymous referee for time and useful comments that improved this work. The work was supported by the *Chandra* ACIS Team (G. Garmire, PI) through SAO grant SV4-74018. G. M. acknowledges contribution from contract ASI-INAF I/088/06/0. This publication makes use of data products from the Two Micron All Sky Survey, a joint project of the University of Massachusetts and the Infrared Processing and Analysis Center/California Institute of Technology, funded by NASA and NSF, and archival data obtained with the *Spitzer Space Telescope*, operated by the Jet Propulsion Laboratory, California Institute of Technology, under a contract with NASA.

APPENDIX

SUPERHOT FLARES

It is difficult to accurately determine temperatures of thermal components $\gtrsim$100 MK from *Chandra* ACIS spectra. To ensure that peak temperatures of $T_{\rm obs,\,pk} > 100$ MK do indeed describe the hottest flare plasmas observed in our sample, we describe checks that have been performed beyond the analysis of Appendix B of Paper I.

For each of the 216 COUP flares treated here, a spectrum was extracted within the total time range $[t_{\rm flare1} - t_{\rm flare2}]$. Spectra were fitted with a WABS $\times$ MEKAL model (for compatibility with Getman et al. 2005) with 0.3 $\times$ solar elemental abundances, and allowing both temperature and column density to be free parameters. The following confirmatory results are obtained. First, for the majority of the flares, the X-ray column densities obtained from the integrated flare spectral fits are in excellent agreement with the source column densities obtained from the full COUP observation by Getman et al. (2005), which we used as fixed parameters during our flare analysis (see also Fig. 16 in Paper I). Second, out of the 73 flares with peak flare temperatures $T_{\rm obs,\,pk} > 100$ MK, only 8 (11%) have integrated flare spectral fits $T_{\rm flare} < 40$ MK, while 80% of the flares with $T_{\rm obs,\,pk} < 100$ MK have $T_{\rm flare} < 40$ MK (Fig. 13). This confirms a distinct difference between superhot and ordinary flares. Third, high-accretion stars[13] have the largest fraction of reported superhot flares: out of a total of 17 flares, nine have peak temperatures $T_{\rm obs,\,pk} > 100$ MK, and another three have temperatures close to 100 MK. This confirms the discussion in § 5 that high accretors preferentially exhibit superhot flares.

Figure 14 further illustrates spectral differences between superhot ($T_{\rm obs,\,pk} > 100$ MK) and ordinary flares. To avoid possible confounding effects of differing absorptions, flare histories, and disk properties, we extract the spectrum within a brief 6 ks interval around

[13] The 12 high-accretion stars with EW(Ca II) < -2 Å are COUP 11, 66, 141, 567, 579, 1044, 1045, 1080, 1096, 1335, 1409, and 1444.

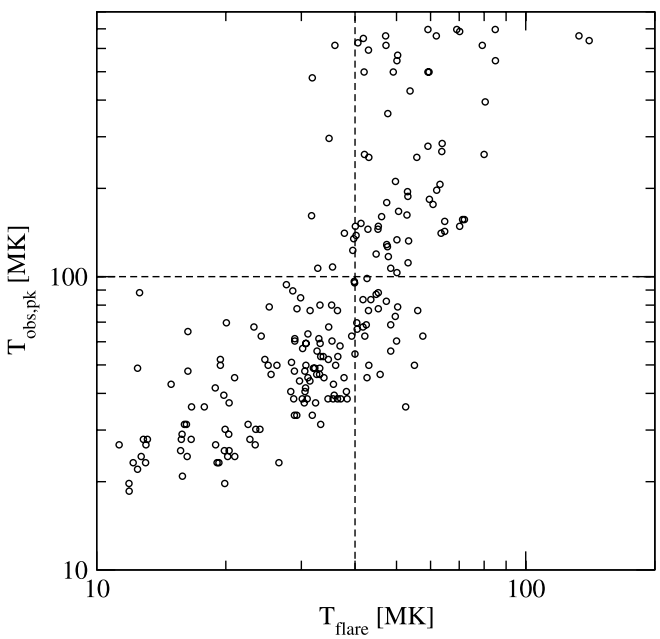

FIG. 13.—For all 216 COUP flares, comparison of the flare peak temperature from MASME analysis (Paper I) with the temperature derived from the spectral fit of the integrated flare spectrum. The horizontal and vertical dashed lines show 100 MK and 40 MK, respectively.

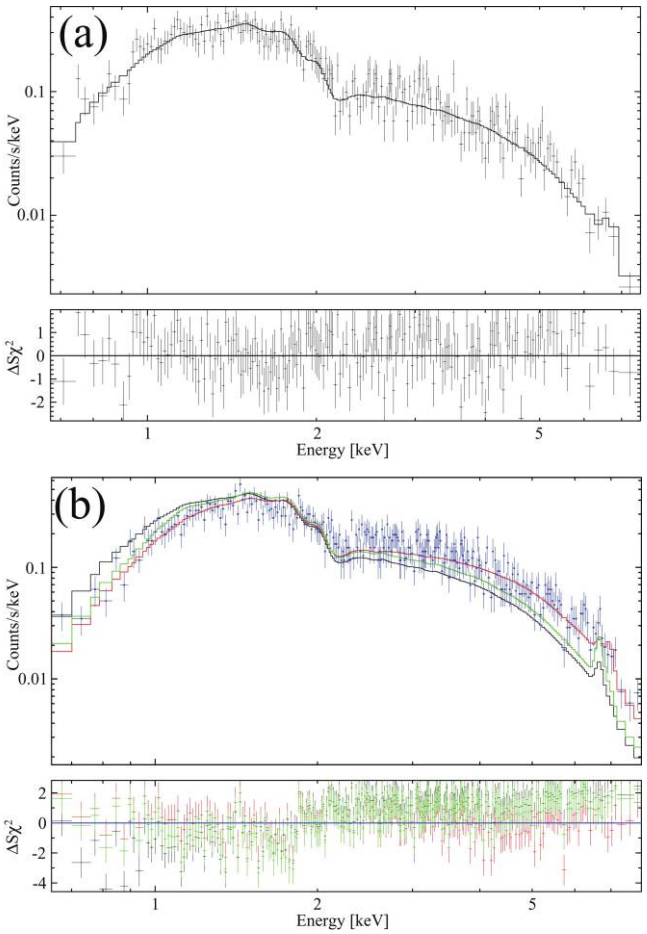

FIG. 14.— Composite flare peak spectra from MIR disk stars with source X-ray column densities in the narrow range of absorption. See Appendix for sample details. (*a*) Composite of 14 ordinary flares from 12 stars with $T_{\rm obs,pk} < 100$ MK. (*b*) Composite of 21 superhot flares from 14 stars with $T_{\rm obs,pk} > 100$ MK. The three spectral models and residuals shown are the ordinary flare model (*black line*), the superhot flare model (*red line*), and the ordinary flare model with $N_{\rm H}$ fixed to that of superhot model (*green line*).

the flare peak for all MIR disk sources in the narrow interval $21.5\ {\rm cm}^{-2} < \log N_{\rm H} < 22\ {\rm cm}^{-2}$. The figure compares combined flare peak spectra for sources with ordinary (Fig. 14*a*) and superhot flares (Fig. 14*b*). Merging these spectra to improve statistical accuracy, the best-fit model parameters of the composite 6 ks spectra are $N_{\rm H} = 4.8^{+0.5}_{-0.5} \times 10^{21}\ {\rm cm}^{-2}$ and $kT = 5.5^{+1.0}_{-0.8}$ keV for the ordinary flares, and $N_{\rm H} = 6.6^{+0.6}_{-0.7} \times 10^{21}\ {\rm cm}^{-2}$ and $kT = 15.2^{+12.1}_{-3.6}$ keV for the superhot flares. The composite spectrum of superhot flares cannot be described by ordinary flare models (compare the black and green lines in Fig. 14*b*). This again demonstrates that superhot flares are the hottest flares of our sample.

REFERENCES

Alef, W., Benz, A. O., & Güdel, M. 1997, A&A, 317, 707
Argiroffi, C., Maggio, A., & Peres, G. 2007, A&A, 465, L5
Arzner, K., Güdel, M., Briggs, K., Telleschi, A., & Audard, M. 2007, A&A, 468, 477
Bally, J., Stark, A. A., Wilson, R. W., & Langer, W. D. 1987, ApJ, 312, L45
Benz, A. O., Conway, J., & Güdel, M. 1998, A&A, 331, 596
Bessolaz, N., Zanni, C., Ferreira, J., Keppens, R., & Bouvier, J. 2008, A&A, 478, 155
Birk, G. T., Schwab, D., Wiechen, H., & Lesch, H. 2000, A&A, 358, 1027
Bouvier, J., Alencar, S. H. P., Harries, T. J., Johns-Krull, C. M., & Romanova, M. M. 2007, in Protostars and Planets V, ed. B. Reipurth, D. Jewitt, & K. Keil (Tucson: Univ. Arizona Press), 479
Bouvier, J., & Appenzeller, I. 2007, IAU Symp. 243 (Cambridge: Cambridge Univ. Press)
Browning, M. 2008, ApJ, 676, 1262
Caramazza, M., Flaccomio, E., Micela, G., Reale, F., Wolk, S. J., & Feigelson, E. D. 2007, A&A, 471, 645
Daou, A. G., Johns-Krull, C. M., & Valenti, J. A. 2006, AJ, 131, 520
Donati, J. F., et al. 2007, MNRAS, 380, 1297
———. 2008, MNRAS, 386, 1234
Drake, J. J., Testa, P., & Hartmann, L. 2005, ApJ, 627, L149
Fárnik, F., et al. 1996, Sol. Phys., 168, 331
Favata, F., Flaccomio, E., Reale, F., Micela, G., Sciortino, S., Shang, H., Stassun, K. G., & Feigelson, E. D. 2005, ApJS, 160, 469
Feigelson, E. D., & Montmerle, T. 1999, ARA&A, 37, 363
Feigelson, E. D., Townsley, L., Güdel, M., & Stassun, K. 2007, in Protostars and Planets V, ed. B. Reipurth, D. Jewitt, & K. Keil (Tucson: Univ. Arizona Press), 313
Feigelson, E. D., et al. 2005, ApJS, 160, 379
Flaccomio, E., Damiani, F., Micela, G., Sciortino, S., Harnden, F. R., Jr., Murray, S. S., & Wolk, S. J. 2003, ApJ, 582, 398
Flaccomio, E., Micela, G., & Sciortino, S. 2006, A&A, 455, 903
Flaccomio, E., Micela, G., Sciortino, S., Feigelson, E. D., Herbst, W., Favata, F., Harnden, F. R., Jr., & Vrtilek, S. D. 2005, ApJS, 160, 450
Forbes, T. G., & Acton, L. W. 1996, ApJ, 459, 330
Franciosini, E., Massi, M., Paredes, J. M., & Estalella, R. 1999, A&A, 341, 595
Franciosini, E., et al. 2007, A&A, 468, 485
Getman, K. V., Feigelson, E. D., Broos, P. S., Micela, G., & Garmire, G. P. 2008, ApJ, 688, 418 (Paper I)
Getman, K. V., Feigelson, E. D., Townsley, L., Broos, P., Garmire, G., & Tsujimoto, M. 2006, ApJS, 163, 306
Getman, K. V., & Livshitz, M. A. 1999, Astron. Rep., 43, 615
———. 2000, Astron. Rep., 44, 255
Getman, K. V., et al. 2005, ApJS, 160, 319

Gregory, S. G., Jardine, M., Cameron, A. C., & Donati, J.-F. 2006a, MNRAS, 373, 827
Gregory, S. G., Jardine, M., Simpson, I., & Donati, J.-F. 2006b, MNRAS, 371, 999
Gregory, S. G., Wood, K., & Jardine, M. 2007, MNRAS, 379, L35
Grosso, N., et al. 2005, ApJS, 160, 530
Güdel, M. 2002, ARA&A, 40, 217
Güdel, M., & Telleschi, A. 2007, A&A, 474, L25
Güdel, M., et al. 2007, A&A, 468, 353
Hartmann, L. 1998, Accretion Processes in Star Formation (Cambridge: Cambridge Univ. Press)
Hartmann, L., Megeath, S. T., Allen, L., Luhman, K., Calvet, N., D'Alessio, P., Franco-Hernandez, R., & Fazio, G. 2005, ApJ, 629, 881
Hayashi, M. R., Shibata, K., & Matsumoto, R. 1996, ApJ, 468, L37
Herbst, W., Bailer-Jones, C. A. L., Mundt, R., Meisenheimer, K., & Wackermann, R. 2002, A&A, 396, 513
Hiei, E. 1994, IAU Colloq. 144, Solar Coronal Structures, ed. V. Rusin, P. Heinzel, & J.-C. Vial (Tatranská Lomnica: VEDA), 163
———. 1997, Mem. Soc. Astron. Italiana, 68, 491
Hillenbrand, L. A. 1997, AJ, 113, 1733
Huenemoerder, D. P., Kastner, J. H., Testa, P., Schulz, N. S., & Weintraub, D. A. 2007, ApJ, 671, 592
Imanishi, K., Nakajima, H., Tsujimoto, M., Koyama, K., & Tsuboi, Y. 2003, PASJ, 55, 653
Isobe, H., Shibata, K., Yokoyama, T., & Imanishi, K. 2003, PASJ, 55, 967
Jardine, M. 2004, A&A, 414, L5
Jardine, M., Cameron, A. C., Donati, J.-F., Gregory, S. G., & Wood, K. 2006, MNRAS, 367, 917
Jardine, M., & Unruh, Y. C. 1999, A&A, 346, 883
Johns-Krull, C. M. 2007, ApJ, 664, 975
Johns-Krull, C. M., Valenti, J. A., Hatzes, A. P., & Kanaan, A. 1999, ApJ, 510, L41
Kahler, S. 1977, ApJ, 214, 891
Kastner, J. H., Huenemoerder, D. P., Schulz, N. S., Canizares, C. R., & Weintraub, D. A. 2002, ApJ, 567, 434
Kopp, R. A., & Pneuman, G. W. 1976, Sol. Phys., 50, 85
Lang, K. R. 1994, ApJS, 90, 753
Long, M., Romanova, M. M., & Lovelace, R. V. E. 2007, MNRAS, 374, 436
Lovelace, R. V. E., Romanova, M. M., & Bisnovatyi-Kogan, G. S. 1995, MNRAS, 275, 244
Luhmann, J. G., Gosling, J. T., Hoeksema, J. T., & Zhao, X. 1998, J. Geophys. Res., 103, 6585
Maggio, A., Flaccomio, E., Favata, F., Micela, G., Sciortino, S., Feigelson, E. D., & Getman, K. V. 2007, ApJ, 660, 1462
Maggio, A., Pallavicini, R., Reale, F., & Tagliaferri, G. 2000, A&A, 356, 627
Massi, M., et al. 2008, A&A, 480, 489
Mathis, J. S. 1990, in ASP Conf. Proc 12, The Evolution of the Interstellar Medium, ed. L. Blitz (San Francisco: ASP), 63
Montmerle, T., Grosso, N., Tsuboi, Y., & Koyama, K. 2000, ApJ, 532, 1097
Mullan, D. J., Mathioudakis, M., Bloomfield, D. S., & Christian, D. J. 2006, ApJS, 164, 173
Osten, R. A., Drake, S., Tueller, J., Cummings, J., Perri, M., Moretti, A., & Covino, S. 2007, ApJ, 654, 1052
Preibisch, T., et al. 2005, ApJS, 160, 401
Priest, E. R., & Forbes, T. G. 2002, Astron. Astrophys. Rev., 10, 313
Prisinzano, L., et al. 2008, ApJ, 677, 401
Ransom, R. R., Bartel, N., Bietenholz, M. F., Lebach, D. E., Ratner, M. I., Shapiro, I. I., & Lestrade, J.-F. 2002, ApJ, 572, 487
Ransom, R. R., Bartel, N., Bietenholz, M. F., Ratner, M. I., Lebach, D. E., Shapiro, I. I., & Lestrade, J.-F. 2003, ApJ, 587, 390
Reale, F. 2002, in ASP Conf. Proc. 277, Stellar Coronae in the *Chandra* and *XMM-Newton* Era, ed. F. Favata & J. J. Drake (San Francisco: ASP), 103
———. 2007, A&A, 471, 271
Reale, F., Betta, R., Peres, G., Serio, S., & McTiernan, J. 1997, A&A, 325, 782
Rebull, L. M., Stauffer, J. R., Megeath, S. T., Hora, J. L., & Hartmann, L. 2006, ApJ, 646, 297
Romanova, M. M., Kulkarni, A. K., & Lovelace, R. V. E. 2008, ApJ, 673, L171
Schmitt, J. H. M. M., Robrade, J., Ness, J.-U., Favata, F., & Stelzer, B. 2005, A&A, 432, L35
Shu, F. H., Najita, J., Ostriker, E., Wilkin, F., Ruden, S., & Lizano, S. 1994, ApJ, 429, 781
Shu, F. H., Shang, H., Glassgold, A. E., & Lee, T. 1997, Science, 277, 1475
Siess, L., Dufour, E., & Forestini, M. 2000, A&A, 358, 593
Simon, T., & Dahm, S. E. 2005, ApJ, 618, 795
Stassun, K. G., van den Berg, M., Feigelson, E. D., & Flaccomio, E. 2006, ApJ, 649, 914
Stelzer, B., Flaccomio, E., Briggs, K., Micela, G., Scelsi, L., Audard, M., Pillitteri, I., & Güdel, M. 2007, A&A, 468, 463
Stelzer, B., Neuhäuser, R., & Hambaryan, V. 2000, A&A, 356, 949
Sturrock, P. A. 1966, Nature, 211, 695
Švestka, Z., Fárnik, F., Hick, P., Hudson, H. S., & Uchida, Y. 1997, Sol. Phys., 176, 355
Švestka, Z., Fárnik, F., Hudson, H. S., Uchida, Y., Hick, P., & Lemen, J. R. 1995, Sol. Phys., 161, 331
Symington, N. H., Harries, T. J., Kurosawa, R., & Naylor, T. 2005, MNRAS, 358, 977
Tsuboi, Y., Koyama, K., Murakami, H., Hayashi, M., Skinner, S., & Ueno, S. 1998, ApJ, 503, 894
Vuong, M. H., Montmerle, T., Grosso, N., Feigelson, E. D., Verstraete, L., & Ozawa, H. 2003, A&A, 408, 581
Wolk, S. J., Harnden, F. R., Jr., Flaccomio, E., Micela, G., Favata, F., Shang, H., & Feigelson, E. D. 2005, ApJS, 160, 423
Yang, H., Johns-Krull, C. M., & Valenti, J. A. 2007, AJ, 133, 73